

MACHINING OF TRANSPARENT BRITTLE MATERIAL BY LASER-INDUCED SEED CRACKS

By

NAVEENKUMAR SHANMUGAM

B.E., Anna University, Coimbatore, INDIA 2011

A THESIS

Submitted in partial fulfillment of the requirements for the degree

MASTER OF SCIENCE

Department of Industrial and Manufacturing Systems Engineering
College of Engineering

KANSAS STATE UNIVERSITY
Manhattan, Kansas

2015

Approved By:

Major Professor
Dr Shuting Lei

Abstract

Transparent brittle materials such as glass and silicon dioxide have begun to replace the conventional materials due to the advantageous properties including high strength and hardness, resistance to corrosion, wear, chemicals and heat, high electrical isolation, low optical absorption, large optical transmission range and biocompatibility. However because these materials are extremely hard and brittle, development of an ideal machining process has been a challenge for researchers. Non-traditional machining processes such as abrasive jet and ultrasonic machining have improved machining quality but these processes typically results with issues of poor surface integrity, high tool wear and low productivity. Therefore a machining technique that overcomes the disadvantages of existing methods must be developed. This study focused primarily on improving the machinability and attaining crack-free machined surfaces on transparent brittle materials by inducing micro cracks or seed damages on the subsurface of the materials. The hypothesis was that micro-cracks induced by femtosecond laser would synergistically assist the material removal process by a cutting tool by weakening or softening the material, followed by conventional machining process. Laser induced damages due to varying laser intensities and at different depths in bulk BK7 glass was studied in order to select the optimal laser machining conditions for the experiments. Dimensional and structural profiles of laser cracks are observed using an optical microscope. A comparative study of machined untreated BK7 samples and damage induced BK7 samples was conducted. Due to its simple process kinematics and tool geometry, orthogonal machining is used for the study. Results showed that machining laser-treated samples caused an average 75% force reduction on comparison to machining of untreated samples. Laser treated machined samples were produced without subsurface damages, and reduced tool wear was noted. Overall improved machinability of BK7 glass samples was achieved.

Table of Contents

List of Figures	v
List of Tables	vii
Acknowledgements.....	viii
Chapter 1 – Introduction	1
Chapter 2 – Literature Review	3
2.1 Current Methodologies of Machining Glass	3
2.1.1 Grinding	4
2.1.1.1 Ultraprecision Grinding	4
2.1.1.2 Chemical Mechanical Polishing.....	4
2.1.1.3 Electrolytic In-Process Dressing.....	5
2.1.2 Chemical Etching.....	6
2.1.3 Lapping	7
2.1.4 Ductile Regime Machining	8
2.1.5 Abrasive Jet Machining	9
2.1.6 Ultrasonic Machining.....	10
2.1.7 Electrochemical Discharge Machining	11
2.1.8 Laser Micromachining	12
2.2 Research Objectives.....	13
Chapter 3 – Preliminary Study of BK7 Glass Milling With Laser Treated Sample	15
3.1 Experimental Setup.....	15
3.1.1 Laser Micromachining	15
3.1.2 End Milling	16
3.2 Results and Discussion.....	17
Chapter 4 – Laser Micromachining	20
4.1 Background.....	20

4.2 Experimental Setup	20
4.3 Preliminary Study of Cracks Profile and Geometry	20
4.3.1 Dimensional Analysis(top view).....	22
4.3.2 Dimensional Analysis(cross-sectional view)	27
4.4 Results and Discussion	32
Chapter 5 – Orthogonal Machining	37
5.1 Background.....	37
5.2 Experimental Setup.....	38
5.3 Results and Discussion	39
5.3.1 Comparison of Cutting Force.....	39
5.3.2 Design of Experiments	40
5.3.3 Surface Integrity.....	44
5.3.4 Chip Morphology	51
5.3.5 Tool Wear	52
Chapter 6 – Conclusions and Future Work.....	54
6.1 Conclusions.....	54
6.2 Future Work.....	54
References.....	55

List of Figures

Figure 1.1 Global sales of glass by application.....	2
Figure 2.1 Schematic diagram of CMP.....	5
Figure 2.2 Schematic diagram of ELID	6
Figure 2.3 Schematic diagram of the lapping process	7
Figure 2.4 Material removal mechanisms in DRM.....	9
Figure 2.5 Micro-ultrasonic-assisted lapping process.....	11
Figure 2.6 Mechanism of ECDM.....	12
Figure 3.1 Schematic of BK7 sample for milling	15
Figure 3.2 Top view of SSD layer forming Groove 4.....	16
Figure 3.3 Tabletop CNC milling experimental Setup	17
Figure 3.4 Comparison of cutting force	18
Figure 4.1 Experimental setup of laser micromachining	21
Figure 4.2 Schematic of BK7 sample and damage zones	21
Figure 4.3 Damage profile	22
Figure 4.4 Crack nomenclature from top-view	23
Figure 4.5 Crack nomenclature cross-sectional view	27
Figure 4.6 Crack profile nomenclature	32
Figure 4.7 Interval plot for groove depth measurement.....	34
Figure 4.8 Groove wall damages from side view of Sample 2	35
Figure 5.1 Schematic of the orthogonal machining process	37
Figure 5.2 Experimental setup of the orthogonal machining process.....	38
Figure 5.3 Average cutting force with standard error bars	41
Figure 5.4 Interval plot for average cutting forces for Experiment I.....	42
Figure 5.5 Interval plot for average cutting forces for Experiment II.....	43
Figure 5.6 Zone classification and nomenclature	44

Figure 5.7 Material removal in untreated sample-top view; depth of cut: 0.1 mm.....	49
Figure 5.8 Material removal in treated sample-top view; depth of cut: 0.1 mm.....	50
Figure 5.9 Material removal in untreated sample: surface classification.....	51
Figure 5.10 Optical images of cutting chips from Machine Test II (depth of cut: 0.2 mm)	52
Figure 5.11 Optical image of flank face tool wear after Machine Test II (depth of cut: 0.2 mm).....	52
Figure 5.12 Optical image of rake face tool wear after Machine Test II (depth of cut: 0.2 mm)	53

List of Tables

Table 2.1 Summary of existing glass machining technologies	3
Table 3.1 Summary of scan layer and associated laser power	15
Table 3.2 Milling conditions	16
Table 3.3 Measured force components	17
Table 3.4 Comparison of machined surfaces	19
Table 4.1 Laser power used for each zone	23
Table 4.2 Regression fit of crack dimensions from top view	25
Table 4.3 Optical images of cracks from top view	26
Table 4.4 Regression fit of crack dimensions from cross sectional view	28
Table 4.5 Optical images of the laser-treated sample from a cross-sectional view with laser beam passing from right to left direction.....	30
Table 4.6 Crack dimensional profile.....	31
Table 4.7 Optical images of laser cracks	34
Table 4.8 Wall damage measurement	35
Table 5.1 Machining parameters.....	37
Table 5.2 Comparison of forces (depth of cut: 0.1 mm; feed rate: 4.23 mm/s)	39
Table 5.3 Comparison of forces (depth of cut: 0.2 mm; feed rate: 4.23 mm/s)	40
Table 5.4 Average cutting force for each trail of experiments	41
Table 5.5 Zone classification for SSD	44
Table 5.6 Damage distribution chart for untreated Machine Test I: depth of cut: 0.1 mm.....	45
Table 5.7 Damage distribution chart for untreated Machine Test II: depth of cut: 0.2 mm	46
Table 5.8 Comparison of machined surface –side view; depth of cut: 0.1 mm	48
Table 5.9 Comparison of machined surface –side view; depth of cut: 0.2 mm	48
Table 5.10 Comparison of machined surface –top view; depth of cut: 0.1 mm	49
Table 5.11 Chip size comparison.....	51
Table 5.12 Maximum flank tool wear.....	53

ACKNOWLEDGEMENTS

I would like to express my sincere gratitude to my advisor Dr. Shuting Lei, for all his encouragement and support throughout the duration of this research. He has been a great inspiration and a great person to work with, always motivating, supporting and guiding me in all my works. It has been a sincere privilege to work under his guidance and learn important things that molded me as a better person.

I would also like to acknowledge Dr. Bradley Kramer, Head of the Department, and the entire Industrial and Manufacturing Systems Engineering Department at KSU for giving me an opportunity to pursue my Masters and making my stay a wonderful learning experience.

I also extend my sincere gratitude and appreciation to Xiaoming Yu, who devoted countless hours and helped me in completing the experiments. I would like to thank my research colleagues Garrick Devin and Hazem Alkotami for their valuable inputs and assisting me in this research.

Finally, I would like to thank my parents, friends and the Almighty who have been a source of confidence, guidance, providing me with all their love and support throughout my life in all my endeavors.

Chapter 1 Introduction

The importance of the transparent brittle materials such as glass and glass ceramics were emphasized by the National Academy of Engineering (NAE-USA), by identifying these materials as the cornerstone to many engineering achievements of the twentieth century [1]. The NAE-USA cited the transformative development of solid state lasers, optical glass fibers and its usage in biomaterials, imaging systems and microelectronic devices. Because of their superior properties, glass and its various forms have replaced traditional materials and are currently used in a range of fields such as aerospace, art, cookware, military, semiconductors fabrication, lighting, health, sensor and pharmaceutical[2]. Flexibility in the compositional design and manufacturing processes of glass has allowed it to become a solution to many challenging engineering problems.

Since 3500 BC, glass has been one of the most prominently used transparent brittle materials [3]. Archaeological evidence suggests that the earliest glass objects were of mid-second millennium BC. Glass continued to be used as a luxury material for making beads and decorated vessels. Although Industrial mass production of glass began in 1887 at Yorkshire, the potential usage of glass in everyday life was not discovered until development of revolutionary float glass in 1960.

Recent emergence of technologies such as solar energy generation has created vast potential for glass applications. From providing chemical and structural support to a photovoltaic cell while transmitting desirable solar radiation to performance of the electrical consumption can be optimized by improving the design of glass units.[1,4] Glass is also used as a substrate for photocatalytic decontamination in solar-driven water purification plants. Borosilicate glass has been used for nuclear waste storage facilities because it provides chemical and mechanical stability to radioactive wastes. Compositions such as Iron phosphate glass have recently been used as replacement of borosilicate glass. Glass also plays an important role in small power supplies, including dielectrics for super capacitors, electrolytes for electrochemical devices, and sealants for high-temperature solid oxide fuel cells. Glass has increasingly been used in micro-fabricated devices such as solid-oxide fuel cells, pumps, optics, electronics, biomedical diagnostics, thermodynamics fluidics reactors, and micro electromechanical systems. Figure 1.1 shows global sales of glass by application.

In the future, glass is predicted to be combined with other materials to expand its application. With increasing sophistication of optoelectronic devices, optical and electronic devices must be combined for applications such as transmission of audio, video and data information [4]. A great challenge for the glass industry is to increase environmental contributions by offering applications to make buildings more energy efficient and ecologically friendly.

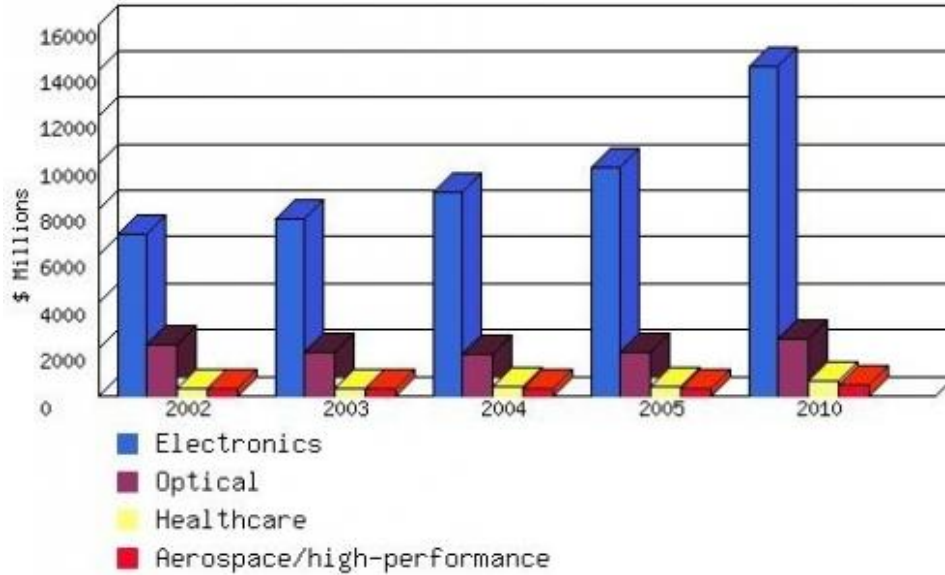


Figure 1.1: Global sales of glass by application [4]

Glass has long-established production methods in basic geometric forms of rods as fibers and filaments, tubes, capillaries, sheets and balls [5]. Although demand for various shapes and complex geometry has risen sharply in relation to glass's growth in application, machining techniques of glass have undergone very little technological development. Cutting, drilling and shaping of glass, quartz and related materials have traditionally been achieved by skilled individuals using cleaving, grinding, polishing or hot-blowing techniques. Non-traditional machining processes such as abrasive jet cutting, ultrasonic machining, laser cutting and electrochemical discharge machining have been introduced in order to address the new requirements.

Existing methodologies to machine transparent brittle materials have unique advantages and disadvantages. Disadvantages include formation of cracked surface and subsurface damages, time consuming operations, and restricted machining depth of cut resulting in low productivity. Therefore, there is an increasing need for improved machining methodologies. This study used laser micromachining in combination with conventional orthogonal machining to harness advantages of both mechanisms for improved machinability. The objective of the research was to conduct a fundamental study of the influence of laser-induced cracks on the machinability of glass in order to determine comparative improvement in surface integrity, reduction in subsurface damages and decreased tool wear. The femtosecond laser micromachining is used to facilitate material removal by inducing damage up to the depth of cut to weaken the sample followed by orthogonal machining to initiate smoother material removal process.

Chapter 2 Literature Review

2.1 Current Methodologies of Glass Machining: Due to their extremely hard and brittle nature, transparent brittle materials, especially glasses, have challenged researchers attempting, to develop an ideal machining process. Conventional glass cutting is done by scoring and breaking using a single point diamond tool [6]. Cutting, grinding, milling, lapping and polishing are commonly employed for machining purposes. Table 2.1 provides an overview of existing glass machining techniques. Various glass machining processes are reviewed in more detail in the following sections.

Table 2.1 Summary of existing glass machining technologies

Methodology	Process description	Drawbacks
Single point diamond turning	Mostly CNC controlled process used in machining optic components	Requires extremely high process control, produces high number of defective parts. used only in specialized applications
Milling, boring and drilling	Conventional milling, boring and drilling processes are used to machine brittle materials such as glass in a CNC controlled process.	Formation surface and subsurface cracks, need of coolant flooding, high tool wear, not suitable for thin wall materials.
Grinding	Typically used for finishing purpose. Process involves rubbing of workpiece against an abrasive material for material removal	Poor accuracy and surface roughness
Chemical Etching	involves controlled chemical dissolution of the workpiece material by contact with a strong acidic or alkaline chemical reagent[17]	Disposal of environmentally harmful chemicals
Lapping	Process involves a rigid metal tool moving under load over a glass surface with abrasive particles suspended in water between them.	High stresses applied causes fracturing leading to poor surface integrity [18].
Ductile regime machining	Conventional machining processes such as milling, turning and grinding are done without breaching the critical depth of cut value to enable material removal in ductile manner resulting in crack free surface.	Low material removal rate.
Abrasive jet machining	high pressurized jet of water/air mixed with abrasives is focused on workpiece to perform material removal	Limitation on machinable part geometry, formation of surface and subsurface damage is noted[26].
Ultrasonic machining	mechanism involves a vibrating tool oscillating at high frequencies supported by abrasive slurry flowing through work piece from tool is used to remove the material	Time consuming, rough surface finish and high tool wear is noted.[27]
Electrochemical discharge machining	Process uses the electrochemical discharge phenomenon by which a high voltage is applied to an electrochemical cell resulting in a discharge between electrode and electrolyte.	difficulty in achieving precision geometry due to lack of sufficient electrolyte flow between tool and work-piece, micro-cracks and thermal damage on machined surface[32]
Laser machining	Uses laser as a heat source to focus at work sample enabling material removal	Formation of heat affected zone and internal stress[35]

2.1.1 Grinding

The grinding is commonly used to finish components in the manufacturing industry. The typical grinding mechanism involves abrasive material rubbing against the workpiece, resulting in material removal. In glass grinding, the abrasive material is typically a diamond with various grain sizes. The grinding process shapes glass by crushing or brittle fracture, and then the cracked surface is machined in the subsequent lapping or polishing process, increasing surface smoothness. Grinding is generally a rough machining method [7], it has the advantage of high material removal rate but accuracy and surface roughness are achieved in finishing processes of lapping or polishing.

Grinding operation in optical glass can be done in three modes based on wheel abrasive grain size and machining depth of cut: - fracture mode, ductile and fracture mode and ductile mode [7]. Ductile mode grinding is made possible by maintaining the grain size less than 20 μm (using diamond wheels) and not breaching the critical depth of cut [7]. As the abrasive grain size and depth of cut increases, the material removal process becomes more brittle.

2.1.1.1 Ultraprecision Grinding

Conventional grinding processes generate poor surface roughness and micro-cracks. In order to improve surface integrity upon grinding, ultra-precision grinding was devised. It was aimed to generate parts with high surface finish, high accuracy and high surface integrity with one machining step [7]. Ultraprecision grinding is done with the machining depth of cut at the submicron level, commonly realized through an abrasive diamond wheel. For optical glass, however results showed that the formation of surface damage and subsurface damage (SSD) are inevitable with ultraprecision grinding. Subsequent abrasive lapping or polishing is required to obtain good surface finish. Therefore, small amplitude root mean square (RMS) values of acoustic emission (AE) signals were applied during machining process resulting in fewer damage patterns and lower damage depth on workpiece [8]. As an extension of the ultraprecision grinding process to aspheric surfaces, Chen et al introduced an ultraprecision aspheric grinding system that can machine large depth-to-diameter ratios of aspheric surfaces [9]. Even under the best conditions, subsurface cracks were inevitable due to the abrasive tool. In addition, the machining process had a very low material removal rate, resulting in low productivity for industrial use.

2.1.1.2 Chemical Mechanical Polishing

The chemical mechanical polishing (CMP) process is primarily comprised of a conditioning head, polishing head and a polishing plate [10]. CMP is a hybrid process that involves chemical etching and free-abrasive polishing. During the process, the workpiece is placed between the rotating polishing plate

and polishing head with rotational and oscillating motion generating a downward force for material removal. The conditioning head supplies the abrasive slurry as shown in Figure 2.1. Although CMP can achieve very low surface roughness upon application to glass materials, the process alters profile accuracy. CMP methods were used to eliminate residual surface defects induced by grinding when making glass disk substrate [11]. However, major challenges of CMP use include (1) obtaining uniform slurry distribution between the pad and workpiece, (2) keeping the pad rough and porous to prevent it from glazing due to plastic deformation of the pad, (3) handling disposal of slurry waste, and (4) making the process economical for usage.

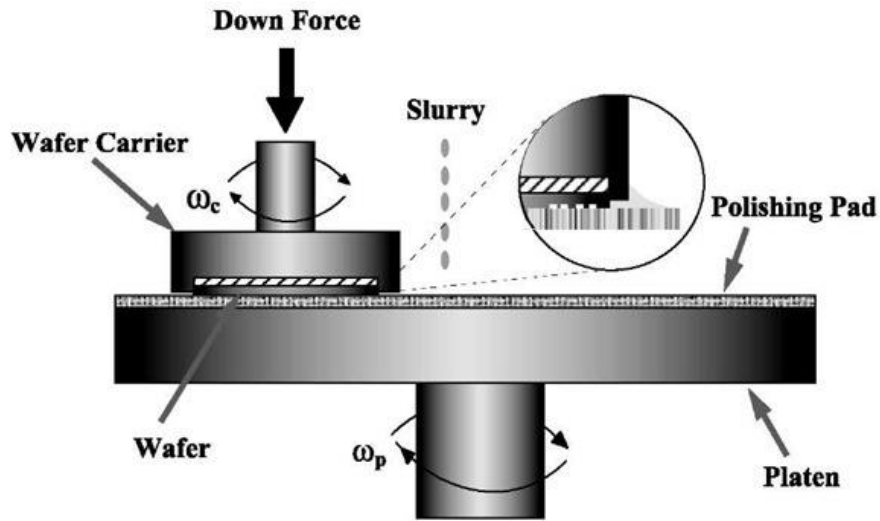


Figure 2.1 Schematic diagram of CMP [12]

2.1.1.3 Electrolytic In-Process Dressing

Wheel truing, glazing, and frequent wheel dressings are the major issues associated with using conventional grinding techniques on machining glass [13]. These issues interrupt the grinding process and reduce productivity. Electrolytic in-process dressing (ELID) grinding, utilizes a metal bonded diamond grinding wheel (anode), a copper or graphite electrode (cathode), a power supply, and an electrolyte, as shown in the Figure 2.2. The electrolyte is dilute aqueous sodium chloride solution with additives of rust resistant chemicals to avoid component damage. The grinding wheel is continuously dressed while the workpiece is machined. During ELID, an insulating film (metal oxide layer) formed on the surface of the wheel, causing the electrical current and the dissolution of the bond material to decrease. During grinding, the oxide layer is worn resulting in the increase of electrical current between the wheel and the electrode and the dissolution of bond material. Due to its self-sharpening property, the ELID process minimizes the problem of wheel loading and glazing, resulting in uninterrupted grinding and a smooth

surface finish. The ELID process was further improved to be suitable for super-abrasive grinding wheels, resulting in decrease grinding force and reduced crack length [14]. Stephenson et al [15] used ELID grinding with AE detection to identify wheel loading and assess the grinding state of a wheel to ensure that optimum grinding conditions were maintained.

The major disadvantage of using ELID is that the metal oxide dissolution and electrolyte solution become contaminated with heavy metal ions, resulting in pollution of the workpiece. In some cases, a solid oxide layer formed along the glass surface. In addition, disposal of electrolyte fluids cause environmental harmfulness.

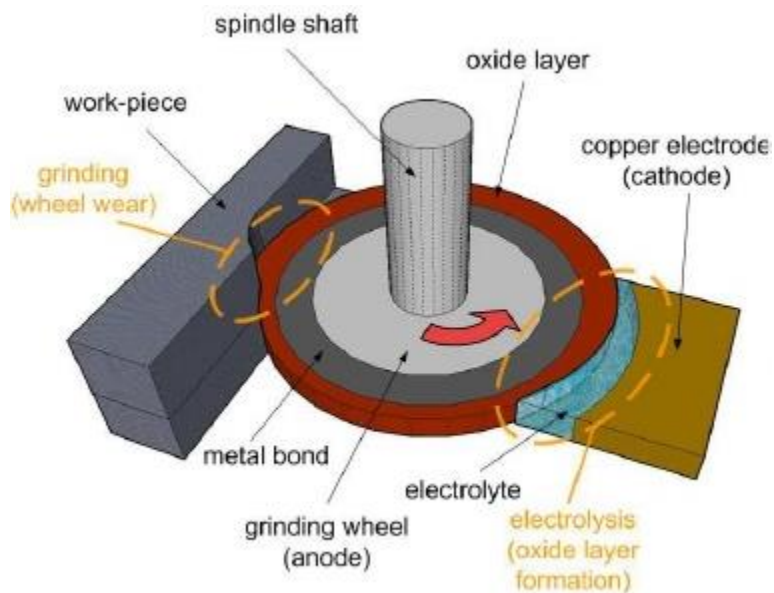


Figure 2.2 Schematic diagram of ELID [16]

2.1.2 Chemical Etching

The chemical etching was developed based on chemical machining principles. Chemical machining involves controlled chemical dissolution of the workpiece material by contact with a strong acidic or alkaline chemical reagent. In principle, chemical machining methodology had its inception in the times of ancient Egypt as early as 2300 BC when it was used to shape copper with citric acid. Until the nineteenth century, chemical etching process was used in decorative purposes. Major industrial application of the chemical etching process began in 1953 when the North American Aviation Inc. used the process to etch aluminum components for rockets. Etching of silicate glasses in aqueous hydrofluoric acid solution is governed by absorption of two reactive species HF and HF_2^- and the catalytic reaction of H^+ ions [17]. A typical chemical etching process follows these steps (1) removing oil, grease, dust or any substance from

the surface of the workpiece, (2) coating the cleaned work piece with a masking material, (3) exposing the area to be chemically etched, (4) carrying out of the etching process primarily by immersion of the workpiece into an etchant bath, and (5) cleaning and removal of masking material

Disadvantages of the chemical etching process include danger in handling due to the use of environmentally harmful chemicals and expensive disposal of those chemicals.

2.1.3 Lapping

Lapping is a machining process, in which two surfaces are rubbed together with abrasives between the surfaces. The aim of the lapping process is to generate as smooth a surface as possible in order to minimize subsequent polishing time. In the lapping process, a rigid iron tool is moved under load over a glass surface, with abrasive particles suspended in water as shown in Figure 2.3. The lapping plate rotates at a low speed (<80 rpm), and a mid-range abrasive particle ($5-20\mu\text{m}$) is typically used for lapping process [18]. In general, the lapping can be classified as: free-abrasive lapping and fixed-abrasive lapping.

Free abrasive lapping occurs when abrasive slurry is applied directly to a lapping plate. Fixed abrasive lapping occurs when an abrasive particle is bonded to a substrate with abrasive lapping films and Silicon Chloride papers. Lapping is a load-controlled process in which the load on the lap is the controlled parameter. The load is transferred to the glass, and the abrasives cause contact between the tool and the glass, resulting in the application of high stresses to the glass and subsequent fracture.

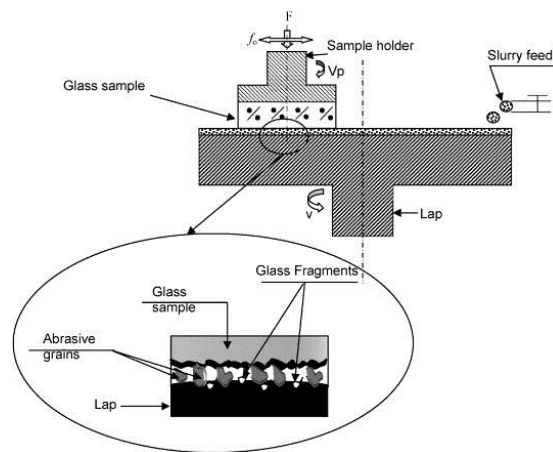


Figure 2.3 Schematic diagram of the lapping process [18]

2.1.4 Ductile Regime Machining

The need for improved surface integrity of brittle materials has been a focus of research topics for the past decades. Because almost all mechanical processes involving tool-workpiece contact inevitably develop subsurface damage, the depth and structure of the near-surface layer influence the mechanical, optical, and electronic performance of components. Effects of SSD include micro-shear bands, micro-ripple patterns, subsurface residual stresses, and various types of microcracks affecting the machined surface quality. DRM was devised to resolve the fracture mode of the material removal process when using conventional machining techniques.

The first investigation of ductile mode machining, which was proposed in 1954, determined that the material removal process was ductile under high hydrostatic pressure during frictional wear of rocky salts. In the 1970s improvements in precision grinding brought about a wide range of brittle materials machined in a ductile manner [19]. In the 1990's precision machining methods such as microturning and micromilling evolved, marking the beginning of ductile regime machining (DRM) techniques. DRM was meant to achieve three important results: machining of crack free high quality surfaces, machining of brittle materials regardless of their hardness factor, and higher productivity rate than polishing processes. DRM assumes that the cutting chip formation undergoes plastic deformation during the material removal process when the depth of cut remains within a critical depth of cut, resulting in formation of a crack-free surface. A critical depth of cut, where plastic removal occurs without fracture, was established. Although many papers have attempted to determine the critical depth of cut to be used in DRM, more sophisticated and advanced calculations are needed to give a better estimation for cutting parameters in DRM.

In one notable study to evaluate the critical depth of cut of DRM, AE energy was generated in the glass grinding to indicate brittle ductile transition; the AE energy was reported to be larger in DRM than in brittle regime machining. As an extension of the DRM technique, ultrasonic vibration assisted DRM was proposed to reduce tool friction [20], and a laser-assisted DRM was investigated [21]-, in which intense heat was used to reduce the yield strength of brittle materials, thereby enabling plastic deformation and resulting insignificantly decreased tool wear. However, critical depth of cut value must not be breached when performing DRM in order to achieve a crack-free surface, otherwise micro-cracks and subsurface damage occur. The other important issue when using DRM is that maintaining the critical depth of cut in the sub-micron level results in a slow material removal rate. Figure 2.4 shows the mechanism of material removal in DRM.

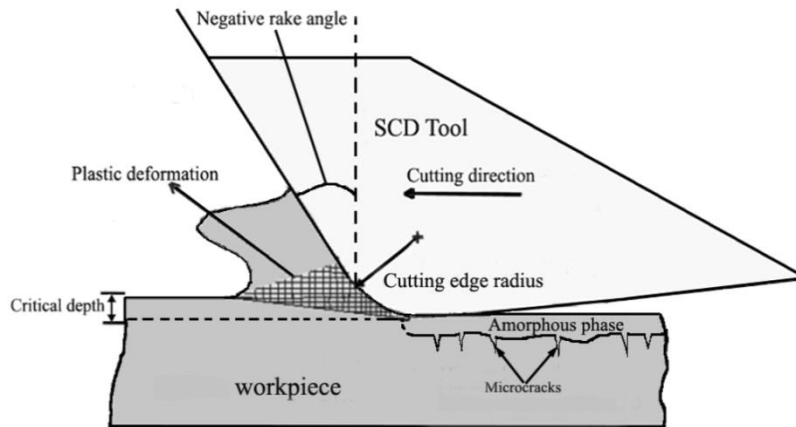


Figure 2.4 Material removal mechanism in DRM [22]

Recently a team of researchers performed ductile mode milling on BK7 glass [42]. The critical depth of cut was determined to be 0.371 μm at cutting speed of 15.7 m/min. Though a high quality surface finish was attained on machined samples, the slow material removal rate remains as a challenge for adopting the process in mass production. It was also identified that increasing the cutting speed affect the machined surface due to thermal softening and viscous relaxation of glass at high temperature. A similar end-milling experiment[43] was done on soda lime glass samples. Removal of material was in ductile mode with good surface quality but the maximum depth of cut used was 2 μm .

Detailed studies have investigated factors affecting DRM, considering tool parameters such as rake angle, tool edge radius, environment and crystallographic orientation of single crystalline materials. Disadvantages of DRM include a ploughing effect on materials and, lack of full comprehension of surface integrity of brittle material[22], In addition, dry versus wet DRM machining is still at the beginning stage of evaluation.

2.1.5 Abrasive Jet Machining

Abrasive water jet machining is one of the most commonly used non-traditional machining methods for machining glass and other brittle materials. Abrasive water jets cut materials at very high pressure using water that contains abrasive grains. Since it is a machining process without physical contact between the tool and the workpiece, the machined surface contains is virtually without any heat affected zone or residual stress [23]. Material removal is due to erosion, but the erosion process usually creates cracked surfaces that cause concern. In a study to address this issue, the brittle fracture of glass in abrasive jet machining was largely credited to the impingement angle of abrasive particles; the angle was controlled at a shallow depth using a stagnation process to produce crack free surfaces. The idea behind was that the

particles should be controlled in order to collide onto a surface at shallow angles and move horizontally at high velocities to keep high removal rates with kinetic energies[24]. Some processes used abrasives and hot air instead of a water jet to perform operations such as drilling, grooving and surface etching [25].

A slow machining rate due to low depth of cut used in machining process was addressed by devising new techniques such as cutting with a forward angling jet cutting plane, multi pass cutting and controlled nozzle oscillation [26]. In the controlled nozzle oscillation technique, a pendulum like nozzle moves forward and backward in the cutting plane at a predetermined frequency, and angular amplitude is superimposed on the typical nozzle transverse motion. This technique improved cutting efficiency, but further study is needed for practical application. High wear rate at the nozzle and mixing tube components, slow machining rates, limitations of the machined product geometry and surface damage occurrences [26] were identified as some of the drawbacks of abrasive jet machining.

2.1.6 Ultrasonic Machining

In the ultrasonic machining (USM), material removal is done via a vibrating tool oscillating at medium to high frequencies supported by abrasive slurry flowing through the workpiece from the tool [27]. Because the tool does not come into contact with the workpiece, minimal heat is generated during the machining process making USM a suitable non-conventional machining technique for glass and other hard materials. The material removal process in USM depends on vibration amplitude, machining load, and the size of abrasive particles. However, conventional USM is time consuming and produces a rough surface finish. Therefore, one research team proposed usage of a low concentration of hydrofluoric acid added to the abrasive slurry, resulting in improved surface quality, but enlargement of the machining hole was identified [28]. Wax coating on the glass substrate [29] was also used to try to enhance surface quality.

As an extension to conventional USM, ultrasonic assisted lapping [30] was formulated to satisfy with increasing needs for high efficiency and precision micromachining of complex work structures. Ultrasonic assisted lapping was implemented by reducing tool diameter, abrasive grains, and vibration amplitude to microscale. Although theoretically ultrasonic assisted lapping showed itself to be a promising micromachining method, deficiency in systematic knowledge on process mechanisms and insufficient optimal process parameters hampers its practical application. In addition, increased tool wear due to its small tool size, small machining load and difficulty in slurry supply due to the capillary effect was noted. Figure 2.5 shows the mechanism of the micro-ultrasonic assisted lapping process.

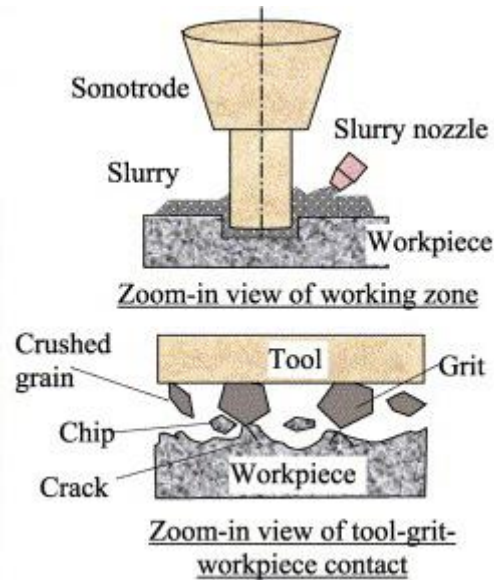


Figure 2.5 Micro-ultrasonic-assisted lapping process[30]

Rotary ultrasonic machining, a hybrid process that combines material removal mechanisms of diamond grinding and USM was employed to improve the material removal rate compared to those obtained by diamond grinding. However, the final surface contained residual fractures and SSD layers.

2.1.7 Electrochemical Discharge Machining

Electrochemical discharge machining (ECDM) was developed to harness the combined advantage of electrochemical machining and electrical discharge machining, such as decreased tool wear and high aspect ratio micro fabrication [31]. ECDM is feasible regardless of electrical conductivity and mechanical hardness of the material. ECDM uses the electrochemical discharge phenomenon by which a high voltage is applied to an electrochemical cell resulting in a discharge between electrode and electrolyte [32]. Application of wire-based electrochemical discharge machining (WECDM) to a non-conductive work piece requires electrical discharge from the circuit between an auxiliary electrode, that is typically comprised of chemically reactive conductors such as graphite and the wire electrode, made usually from metals with low electrical resistance such as brass. Although WECDM is considered an effective method of machining, its effectiveness depends on the spark discharge because it becomes ineffective with increased depth of cut. Difficulty in achieving precision geometry was also noted with lack of sufficient electrolyte flow between tool and work-piece. Many researchers have tried to address these shortcomings. In a notable work, magnetic field assisted ECDM [33] successfully enhanced the electrolyte flow. In addition, the randomness of gas film formed around the tool electrode during the machining process resulted in excessive overcut of the materials, thereby affecting the accuracy negatively. In order to counter this excessive undercut due to increased voltage and wire vibration in WECDM which affected

the shape accuracy, one researcher suggested the addition of SiC abrasives to the electrolyte [34]. As the need for ultraprecision products rose, micro-ECDM was devised.

Micro-ECDM was developed to improve low surface integrity because of high working voltage and long reactive tool length caused by WECDM. Typical working voltage significantly increases the discharge current resulting in micro cracks and thermal damage on the machined surface. Many approaches have been tried to lower working voltage in the ECDM process, including reducing the gas film thickness and enhancing electric field intensity between the tool surface and the adjacent electrolyte. In one such approach, a surface textured tool was proposed to reduce working voltage by enhancing electric field intensity around the tool surface in micro electrochemical discharge cutting of glass [31]. Figure 2.6 shows a setup for the ECDM process.

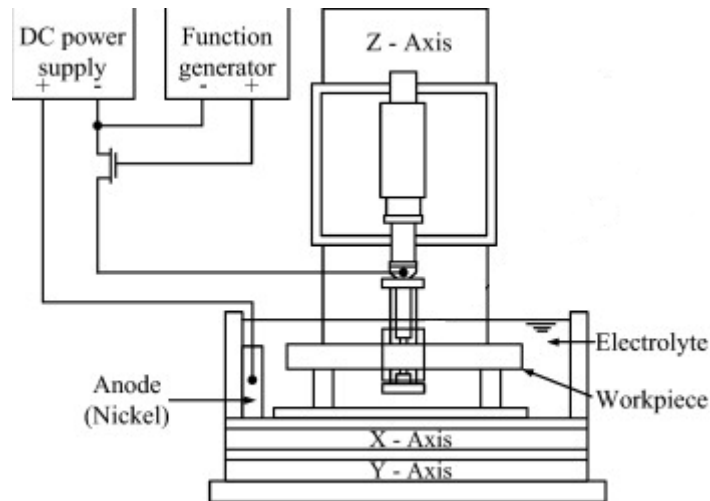


Figure 2.6 Mechanism of ECDM [31]

2.1.8 Laser Micromachining

A laser is one of the most important tools in modern applications because of its unique properties such as high intensity electromagnetic flux, monochromaticity and high spatial and temporal coherence [35]. Laser beams can be focused to a very small area with very high radiance thereby acting as a heat source and enabling melting or boiling of the focused material. Material removal occurs by melt ejection, vaporization or ablation. In general laser micromachining uses ultrashort laser beams to acquire an exceptional degree of control without generating damage to the surrounding area. It involves inducement of ultra-small features on or inside the surface of the material. Because the laser energy is deposited at a time scale that is much smaller than the heat transmission and electron-photon coupling, no damage occurs outside the intended zone.

Researchers have used a laser as the heat source for thermally assisted machining of glass and other transparent brittle materials to elevate the work piece temperature at the cutting zone in order to facilitate material removal [36]. Lasers have also been used to induce thermal stress cleavage for separating thin wafers from brittle materials such as silicon, glass and ceramics. Induction of compressive stress during laser heating was followed by water-jet cooling for crack initiation and material removal occurred due to laser assisted material removal processes in silicate glass [38].

Ultrashort laser pulses were used to write optical waveguides, creating optical breakdown and structural changes in bulk glass, in research that focused on optics and memory storage disks [37]. Lasers were used as an important tool for hybrid machining .Hybrid machining involves two processes in which either both processes are directly involved in material removal or only one is directly involved and the other assists in the material removal process. The hypothesis in laser/water jet cutting is that both processes work synergistically to remove material through thermal-shock fracturing [39]. The laser is initially used for heating to create temperature difference immediately followed by rapid quenching using a low pressure water jet, causing thermal stress that eventually leads to fracture.

2.2 Research Objectives

The goal of this research was to improve the machinability of transparent brittle materials with the assistance of laser-induced damage inside the material. This study contained the following specific objectives:

- 1) Study the fundamental effect of laser induced damage on machining of BK7 glass.
- 2) Characterize femtosecond laser induced damage profile with regard to laser parameters.
- 3) Design an experimental setup and conduct experiments for orthogonal machining of BK7 glass.
- 4) Compare and analyze results of experiments conducted between a sample with damage and an untreated sample based on surface integrity, tool wear, and cutting force.

The remainder of this thesis is organized into descriptive sections. Chapter 3 describes a preliminary study of milling experiments conducted on a damage-induced BK7 sample. Chapter 4 explains laser micromachining and provides analysis of damage layer formation and crack profiles. The experimental setup of orthogonal machining experiments are discussed and comparative results based on surface integrity, tool wear, and cutting force data are analyzed in Chapter 5. Conclusions and future work are discussed in Chapter 6.

Chapter 3 Preliminary Study of BK7 Glass Milling with Laser treated Samples

3.1 Experimental Setup

3.1.1 Laser Micromachining

A preliminary study was conducted to understand the effect of laser treatment on machining of transparent brittle materials. A femtosecond laser beam delivered from a Ti-Sapphire laser (Kansas Light Source, J.R. Macdonald Laboratory) was used for the laser treatment. The laser beam had 25-fs pulse duration (full-width-at-half-maximum, FWHM), 790-nm center wavelength, 2-kHz repetition rate, and 2-mJ maximum pulse energy. A circular BK7 sample 25.4 mm in diameter and 6 mm in thickness was modified with five equally spaced lines of subsurface laser treated scan layers as shown in Figure 3.1. Each line had multiple layers of laser scanning performed at varying intensities and depth, as shown in Table 3.1. The width of each subsurface scan line was 3.175 mm, equal to the diameter of the milling tool used. Figure 3.2 shows an image of Groove 4 taken using an optical microscope.

Table 3.1 Summary of scan layer and associated laser power

Groove No	Laser Power, mW	Scan Layer Depth, mm
1	400	0.55
2	600	0.55
	450	0.475
	330	0.4
	230	0.325
3	700	0.55
	500	0.475
4	600	0.55
	450	0.475
	330	0.4
	230	0.325
5	550	0.55
	400	0.475
	270	0.4
	170	0.325

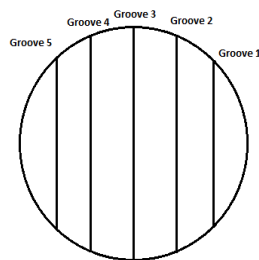


Figure 3.1 Schematic of damage pattern

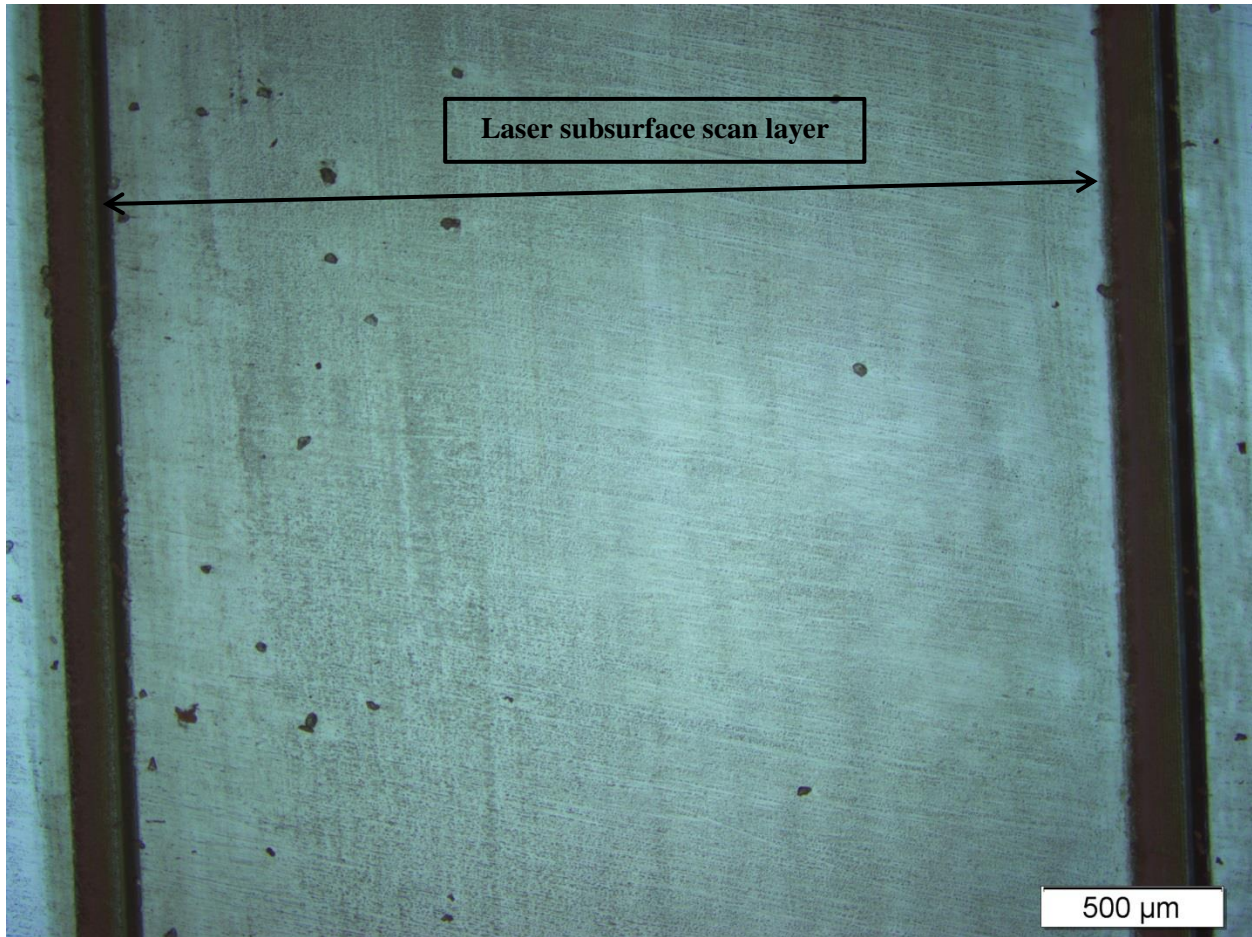


Figure 3.2 Top view of SSD layer forming Groove 4

3.1.2 End Milling

Micro-grain tungsten carbide end mills were used to machine five grooves over the laser treated subsurface layers. Table 3.2 shows milling parameters used for the experiments. As shown in Figure 3.3, the workpiece was mounted on a fixture that was mounted on a Kistler three-component dynamometer in order to collect cutting forces. A Kistler dual-mode charge amplifier was used to amplify signals of the cutting forces measured by the dynamometer. The computer data acquisition system was controlled by LabVIEW.

Table 3.2 Milling conditions

MILLING CONDITIONS	
Feed rate	0.35 mm/rev/tooth
Cutting speed	1.3 m/s
Depth of cut	0.5 mm



Figure 3.3 Tabletop CNC milling experimental setup

For comparison, milling operations with the same conditions as mentioned in Table 3.2 were conducted done on an untreated side of the BK7 sample.

3.2 Results and Discussion

Cutting force data collected by LabVIEW were processed and analyzed. Table 3.3 shows average cutting force values for the laser treated and untreated samples.

Table 3.3 Measured force components

Average Force in N, Untreated Side			Groove	Average Force in N, Laser-treated Side		
Feed Force	Thrust Force	Main Force		Feed Force	Thrust Force	Main Force
2.562	0.843	2.473	1	1.222	1.997	4.271
			2	2.707	1.427	4.254
			3	1.357	0.529	2.268
			4	0.755	0.753	1.295
			5	0.853	1.96	1.43

The milling experiment on the untreated side was repeated three times in order to obtain average force values. However, analyzed force data did not show clear indication on the effect of laser induced damages. Although no consistent reduction in cutting force was evident while machining treated samples compared to untreated samples, indications of substantial difference in force values were observed, shown

in Figure 3.4. In feed force comparison, almost all the grooves except Groove 2 demonstrated reduced cutting force compared to the untreated one. For main Force, grooves 3,4, and 5 had reduced cutting forces. Table 3.4 shows a comparison of machined surfaces, but limited difference is evident.

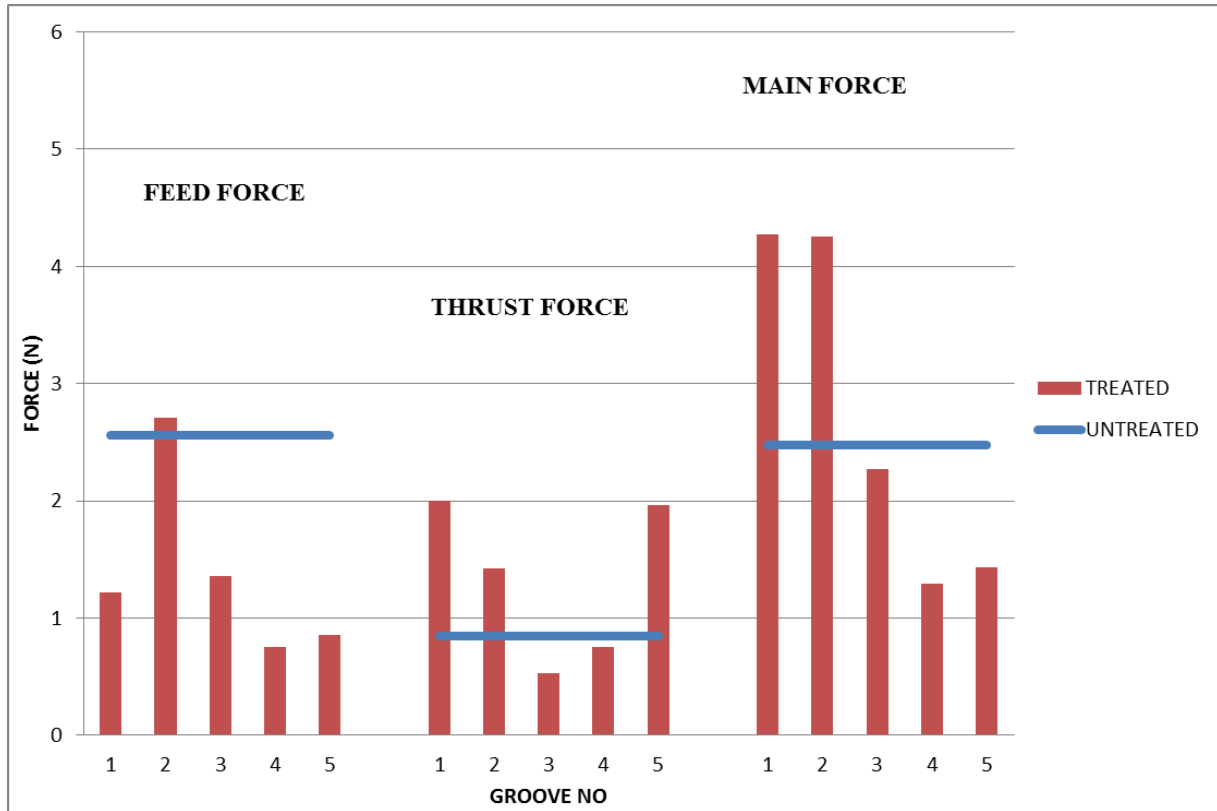


Figure 3.4 Comparison of cutting force

In summary, this preliminary study provided mixed results in terms of the effect of laser treatment on cutting force, demonstrating need for further studies to establish the effect of laser treatment on machining. In order to have better control of the process, the decision was made to pursue the study with orthogonal machining technique which has a relatively simpler tool geometry and process kinematics.



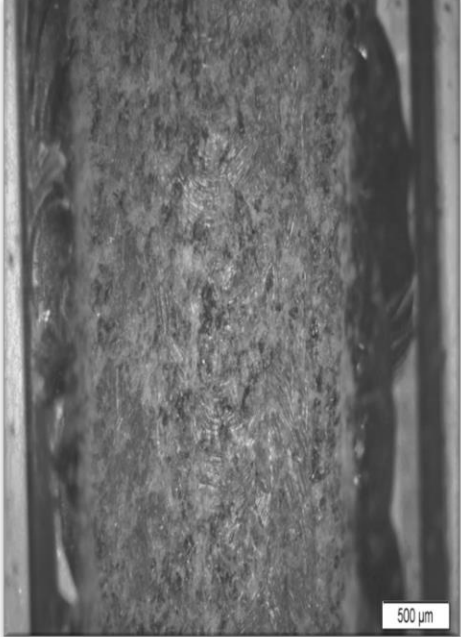

Laser-treated Machined Groove	Untreated Machined Groove
 <p>A scanning electron micrograph (SEM) showing the surface of a laser-treated machined groove. The surface is dark and exhibits a highly textured, porous appearance with irregular, interconnected features. A scale bar in the bottom right corner indicates 500 μm.</p>	 <p>A scanning electron micrograph (SEM) showing the surface of an untreated machined groove. The surface is lighter in color and appears smoother than the laser-treated surface, with some visible machining marks and a less porous structure. A scale bar in the bottom right corner indicates 500 μm.</p>
 <p>A scanning electron micrograph (SEM) showing the surface of a laser-treated machined groove. The surface is dark and exhibits a highly textured, porous appearance with irregular, interconnected features. A scale bar in the bottom right corner indicates 500 μm.</p>	 <p>A scanning electron micrograph (SEM) showing the surface of an untreated machined groove. The surface is lighter in color and appears smoother than the laser-treated surface, with some visible machining marks and a less porous structure. A scale bar in the bottom right corner indicates 500 μm.</p>

Table 3.4 Comparison of machined surfaces

Chapter 4 Femtosecond Laser Micromachining

4.1 Background

Femtosecond lasers are commonly used for micromachining because they create minimal damage and limited heat-affected zones outside the intended focus area. Unlike lasers with long pulse duration, femtosecond lasers deposit energy into the material in a very short time, thus minimizing energy loss to surrounding areas.

Intensity in the focal volume of workpiece can become high enough to cause nonlinear absorption. When the absorption is strongly non-linear, material breakdown can be localized in the focal volume inside the bulk of glass without affecting the surface. Therefore, a femtosecond laser was used to induce damage to glass workpieces in this study.

4.2 Experimental Setup

Borosilicate glass schott samples (BK7) were used as workpiece materials for the experiments for this study. The damage in bulk BK7 glass is induced with a femtosecond laser system (Kansas Light Source, J.R. Macdonald Laboratory). The laser beam had 25-fs pulse duration (FWHM), 790-nm center wavelength, 2-kHz repetition rate, and 2-mJ maximum pulse energy. The beam diameter ($1/e^2$) was measured to be 9.8 mm with the knife-edge method. Laser power was adjusted with a combination of a half-wave plate and a polarizer. A plano-convex lens with 200-mm focal length was used to focus the beam on the sample surface. The focal spot diameter ($1/e^2$) was estimated to be 20 μm . The sample was mounted on a motorized three-dimensional stage (Newport ILS100PP) as shown in Figure 4.1.

The position of the focus was determined to be the brightest portion of plasma filament formed with input power, measured before the lens with a power meter. A CCD camera mounted with a 20 \times , 0.3NA objective lens was placed perpendicular to the laser propagation direction and was used to monitor positions of laser focus and sample surface.

4.3 Preliminary Study of Cracks Profile and Geometry

First, decision was made to study laser-induced cracks and understand the structural and dimensional profile of the crack. A circular BK7 glass sample with a diameter of 25.4 mm and a thickness of 2 mm was prepared to be treated with a femtosecond laser. The surface area of the sample was divided into three zones, as shown in Figure 4.2.

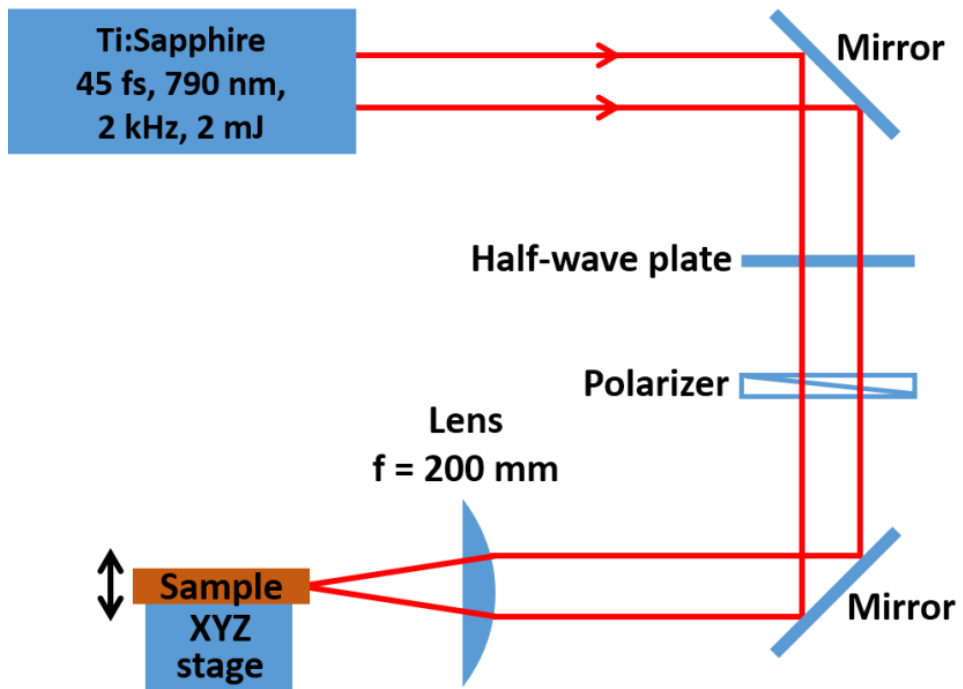


Figure 4.1 Experimental setup of laser micromachining.

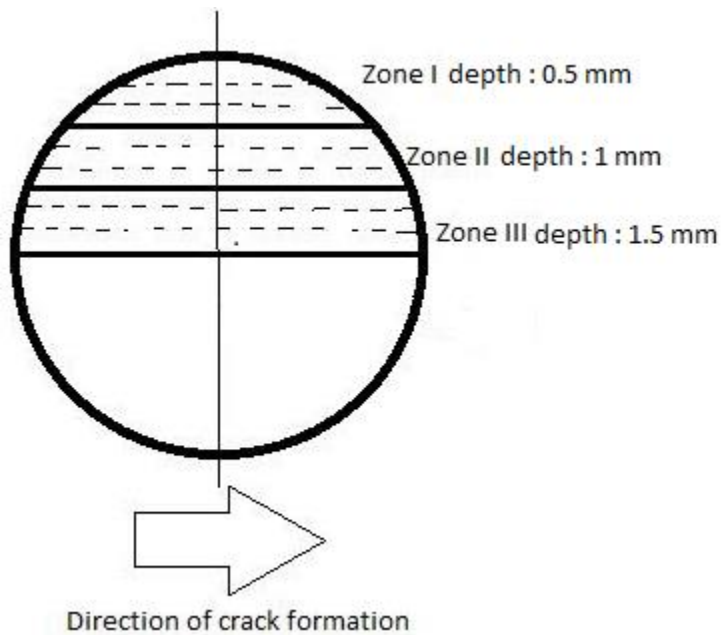


Figure 4.2 Schematic of BK7 sample and damage zones

Upon laser treatment, the sample was bisected into two symmetrical halves perpendicular to the direction of crack formation – (i.e., each half of the sample encamped one half of each zone) in order to study the cross-sectional crack profile using an optical microscope.

Damage orientation seen from the top surface is shown in Figure 4.3. Each line of damage was separated by a distance of 100 μm and each damage spot was separated from the subsequent damage spot by a distance of 25 μm . Each zone was treated with a laser beam of varying power. The laser power for each zone is given in Table 4.1.

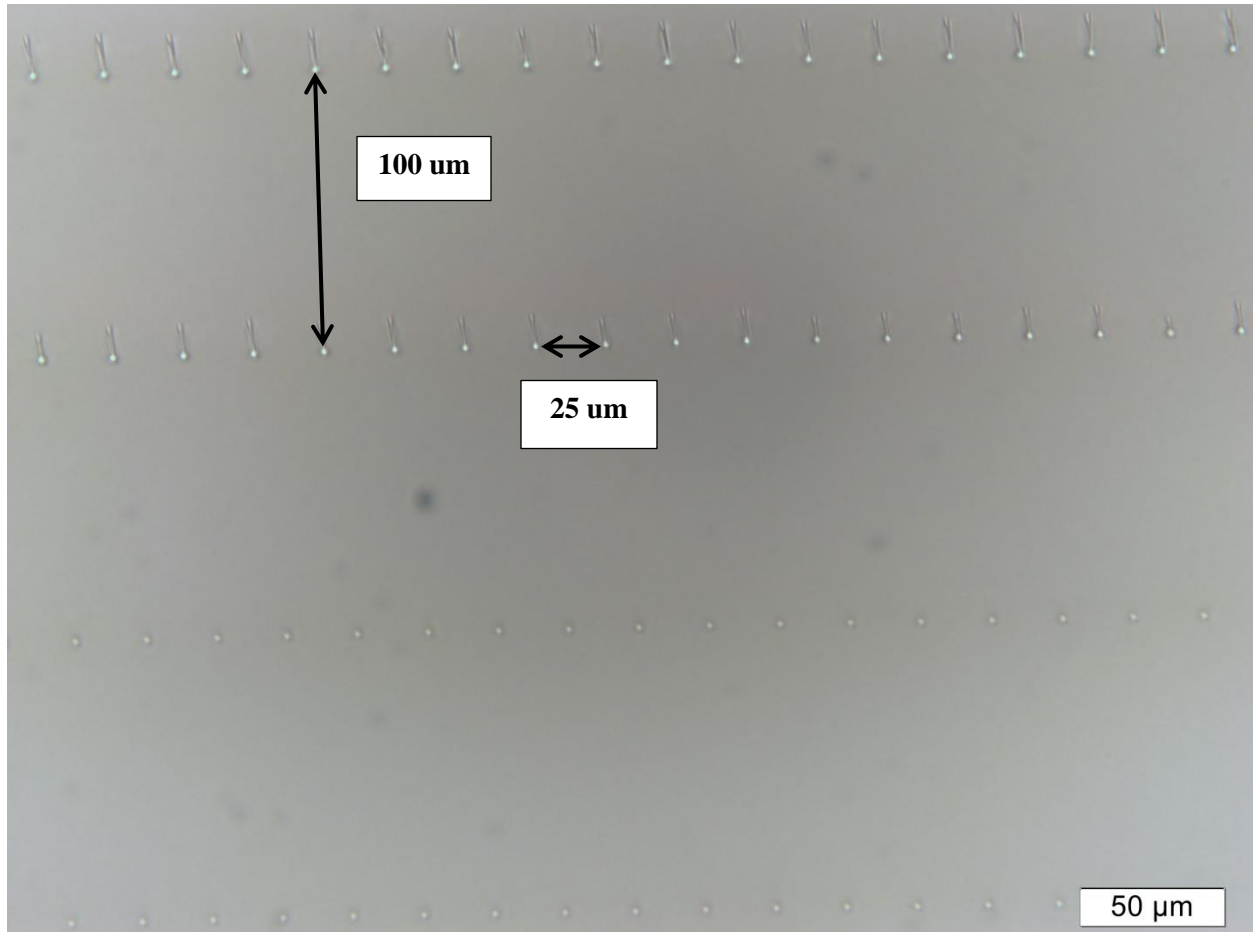


Figure 4.3 Damage profile

4.3.1 Dimensional analysis (top view)

Dimensional analysis of the cracks was conducted in order to study damage caused by lasers with varying power and at different depths from the sample surface. For each laser power at every zone, a sample size of 10-12 individual damage spots were chosen and the average of its linear crack spread dimensions, area of the crack spread, and angular orientation of the cracks were measured. Cracks were analyzed and documented using pictures from the top view and cross sectional view. The purpose of this analysis was to learn about and predict crack size for specified laser power and specified depths. Dimensional analysis from the top view provided the profile of lateral spread of cracks.

Table 4.1 Laser power used for each zone

Laser Power, W		
Zone 1	Zone 2	Zone 3
0.50	0.50	0.50
0.05	0.05	0.05
0.10	0.10	0.10
0.15	0.15	0.15
0.20	0.20	0.20
0.25	0.25	0.25
0.30	0.30	0.30
0.35	0.35	0.35
0.40	0.40	0.40
0.45	0.45	0.45
0.50	0.50	0.50
0.55	0.60	0.60
0.60	0.70	0.70
0.70	0.80	0.80
0.80	0.90	0.90
0.90	1.00	1.00
1.00	1.10	1.10
1.10	1.20	1.20
1.20	1.30	1.30
1.30	1.40	1.40
-	1.50	1.50
-	1.60	1.60
-	1.70	1.70
-	-	1.80
-	-	1.90
-	-	2.00
-	-	2.10

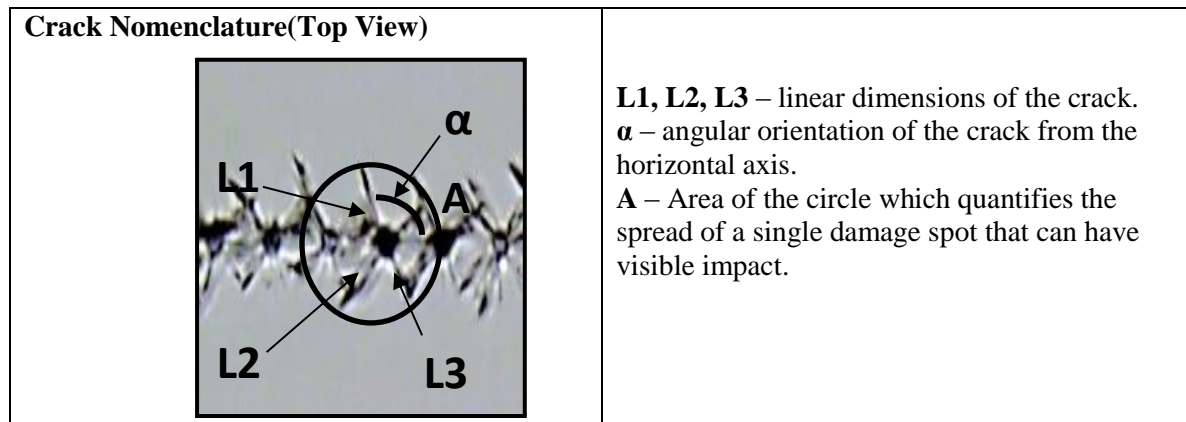
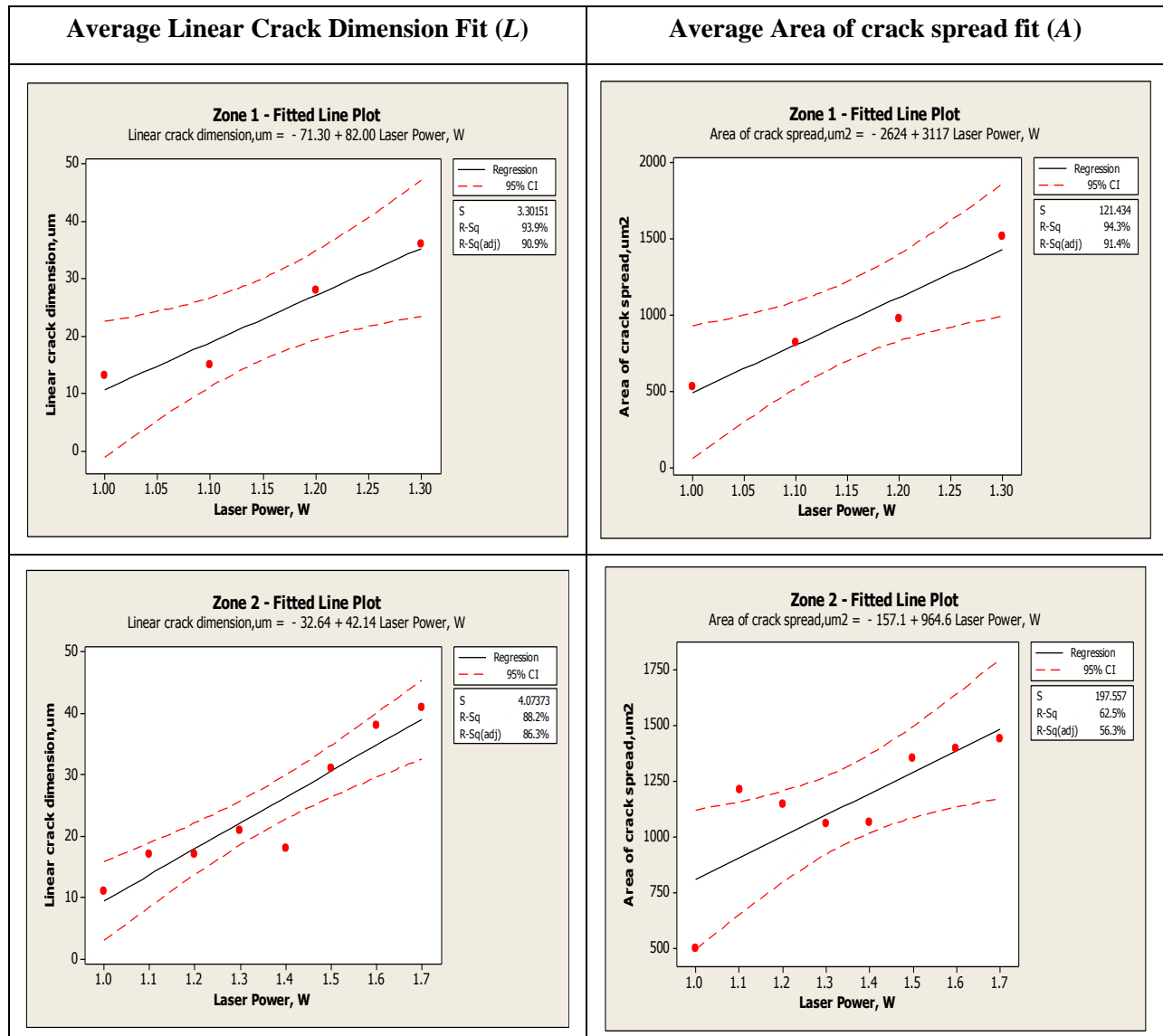
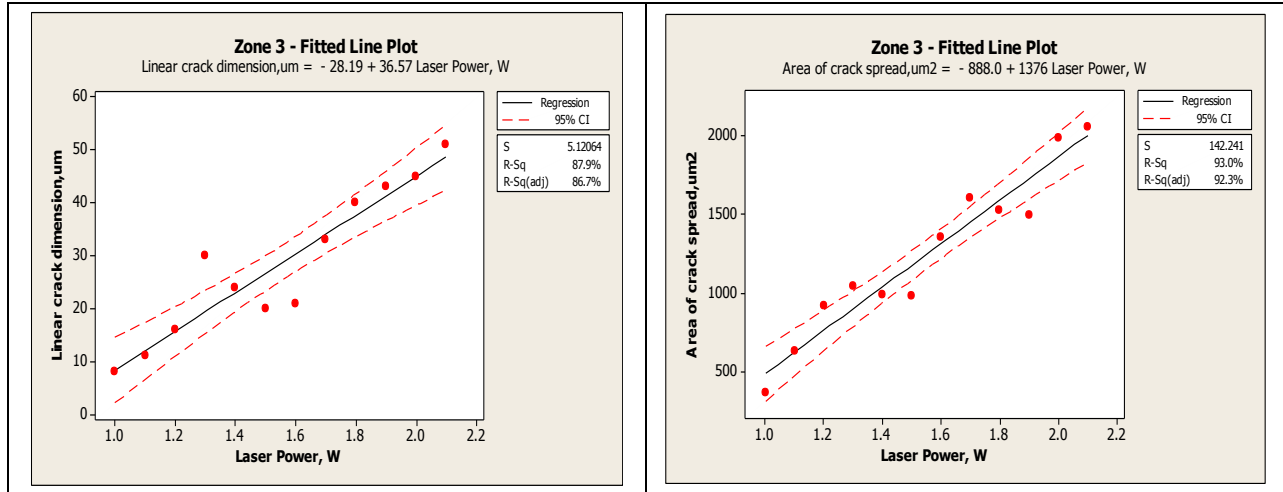


Figure 4.4 Crack nomenclature from top-view

A sample of individual cracks between 10 and 15 observations for each power at all three zones was measured using attributes shown in Figure 4.4. Linear cracks labelled as L1,L2...Ln were added together as the total linear crack dimension, L . For each laser power at every zone, the average of the total linear crack dimension, L was calculated using sample observations. Similarly, the average area of the crack spread A , was determined for all powers in every zone. The angular value α , was measured in order to understand the angular orientation of the crack spread.

Table 4.2 Regression fit of crack dimensions from top view

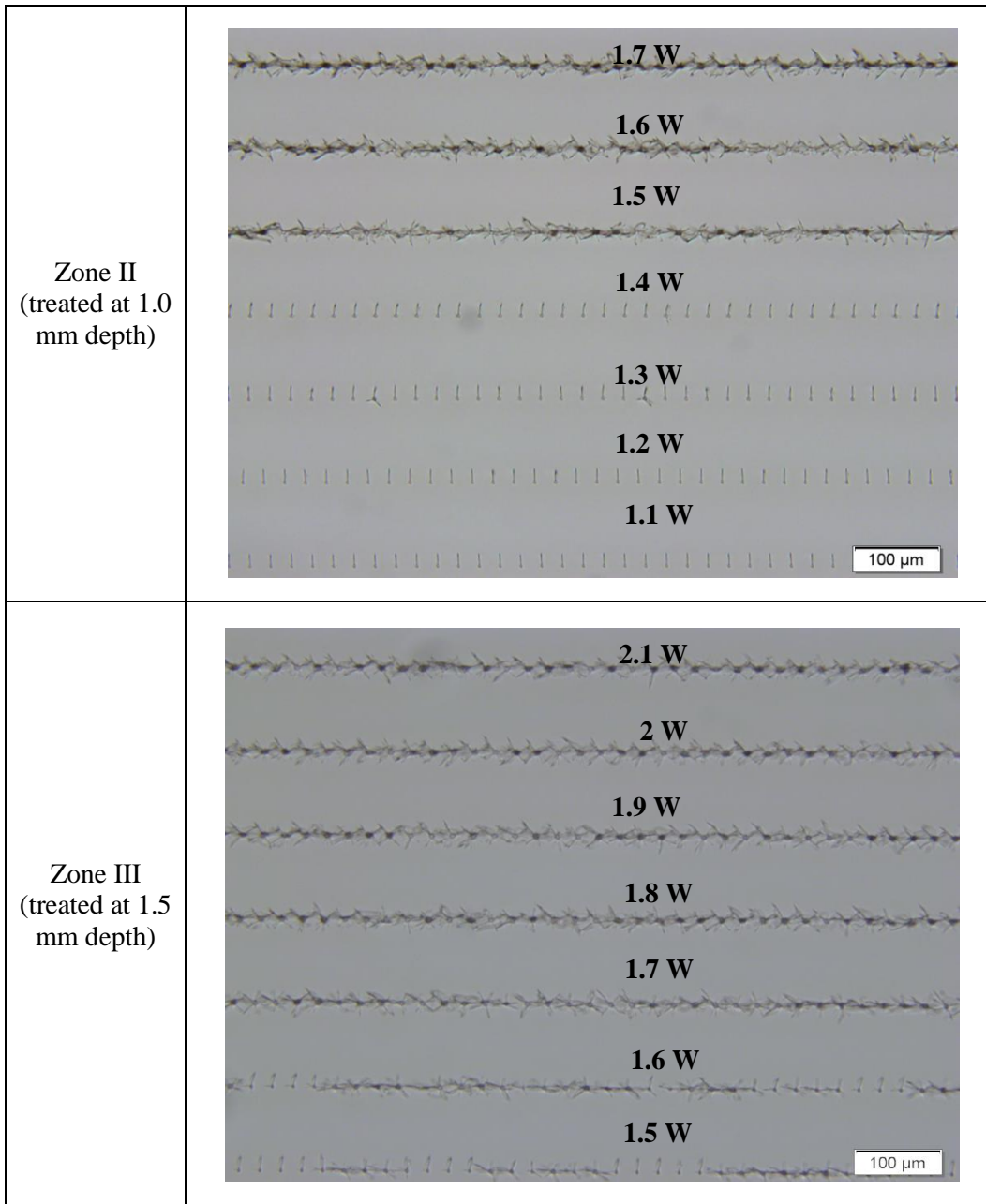




In Table 4.2, the average crack linear dimension, L and the area of the crack spread, A are fitted against laser power in all three zones. According to results in the table, the dimension and spread of cracks increased with power. For a given power such as 1W, the average linear crack dimensions were 13 μm , 11 μm , and 8 μm for Zone I, Zone II, and Zone III respectively. For a given laser power, the average crack dimension and area of the crack spread decreased with increased material depth. A fitted regression linear equation with a confidence interval at 95% significance level was derived to map crack dimensions and its spread for corresponding laser power in each zone.

Table 4.3 optical images of cracks from top-view

Description	Laser Cracks (top view)- with Labelled Laser Intensities
Zone I (treated at 0.5 mm depth)	



Optical images of cracks with labelled laser powers from top-view are shown in Table 4.3. In Zone I, laser power higher than 1W produces visible cracks which were taken into consideration for dimensional analysis. Negligible structural modification was observed for laser power less than 1W in all three zones and no visible crack geometry was evident to be considered for dimensional evaluation. Also, each crack was not connected to the subsequent one for laser power less than 1.2W in Zone I, 1.5 W in Zone II and 1.5 W in Zone III.

4.3.2 Dimensional Analysis (cross-sectional view)

After analyzing the cross section of the sample, the length of cracks propagating beyond the intended damage depth was determined. It provides important information because these cracks tend to propagate beyond the intended damage spot. With high laser power, the crack was long, but it was also dependent on intended depth of the damage. The aim of this study was to achieve minimal propagation of crack into the material from the intended damage spot. Cracks that propagate beyond the intended depth reduce product quality, resulting in poor surface integrity. However, with predication of crack profile for the given laser power and damage depth, adjustments were made to the intended damage spot so that no laser-affected crack zone occur beyond the machining depth of cut. The length of damage, l propagating beyond the intended depth, as shown in Figure 4.5 was measured for all laser powers that produce visible cracks at every zone.

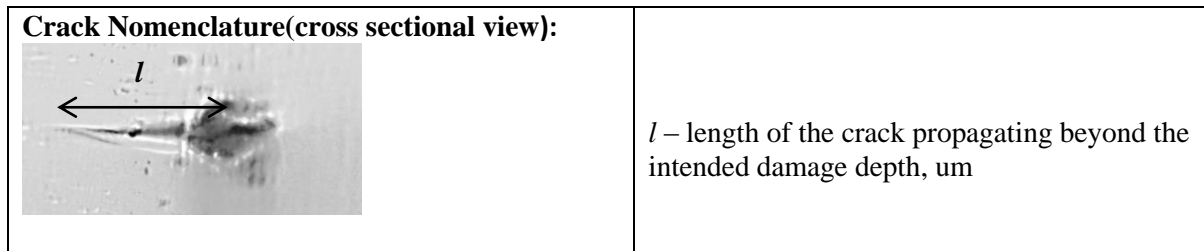
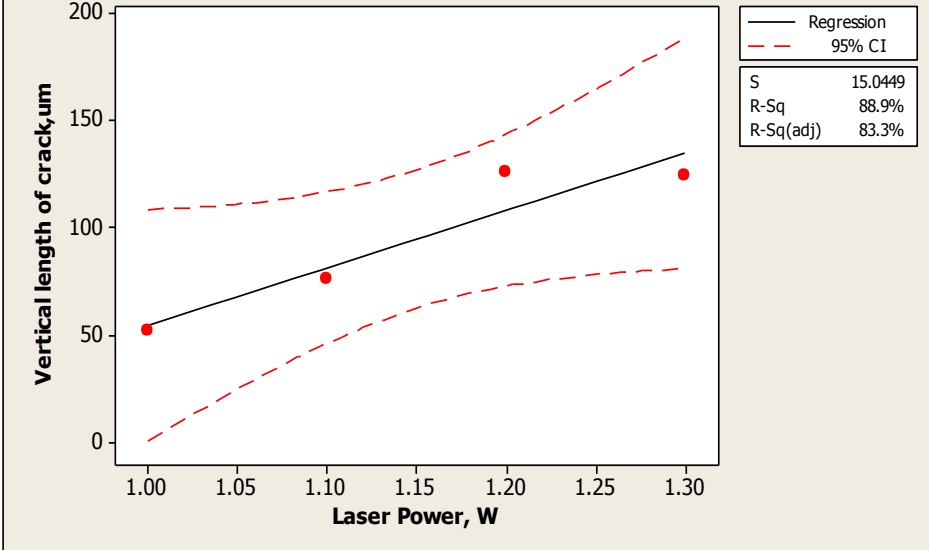
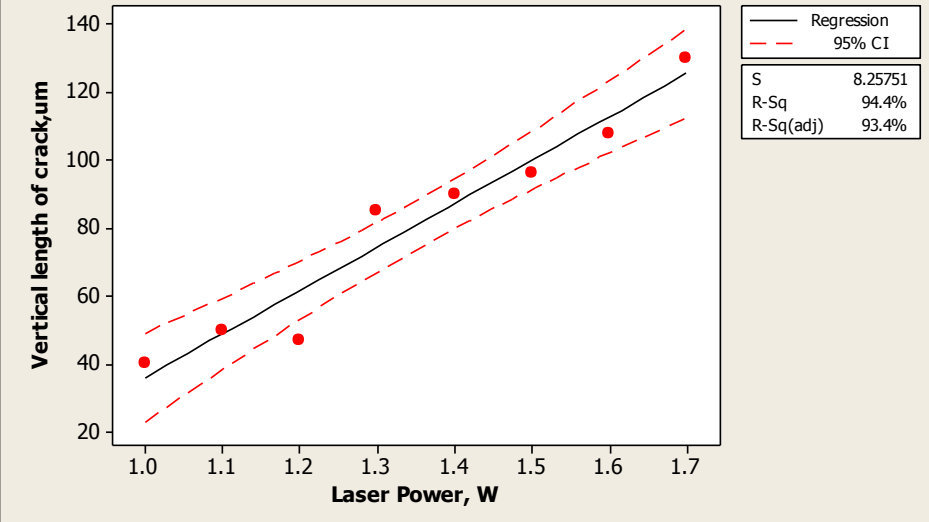


Figure 4.5 Crack nomenclature cross-sectional view

Length of cracks measured in micrometers (μm) was plotted against laser power for each zone. In Table 4.4, vertical propagation of the cracks was fitted with a regression model against laser power at 95% confidence interval. For example, lengths of vertical propagations of cracks created by laser power of 1W were 50 μm , 40 μm , and 20 μm at Zone I, Zone II, and Zone III respectively. For a given power, the length of crack propagation decreased with increased material depth. Maximum crack propagation of 160 μm was noted at the maximum laser power of 2.1 W in Zone III.

Propagation of damage beyond the intended spot creates a major bottleneck in machining brittle materials. Often breaches the intended depth of cut for subsequent machining experiments creating cracked surfaces. One way to counter crack propagation is to factor it before choosing damage depth. For example, in order to create a crack layer at 1 mm depth in bulk material using 1W of laser power, the focus spot should be $1.5 - 0.04 = 1.46$ mm to prevent the presence of laser induced cracks after machining. However, a crack may not propagate to the same dimension every time and the effect on machining with such consideration must be analyzed.

Table 4.4: Regression fit of crack dimensions from cross sectional view

Description	Length of Crack Propagating Beyond Intended Spot										
<p>Zone I (treated at 0.5 mm depth)</p>	<p style="text-align: center;">Zone 1 - Fitted Line Plot</p> <p style="text-align: center;">Vertical length of crack,um = - 214.6 + 269.0 Laser Power, W</p>  <table border="1" data-bbox="1230 443 1409 583"> <tr> <td>—</td> <td>Regression</td> </tr> <tr> <td>- - -</td> <td>95% CI</td> </tr> <tr> <td>S</td> <td>15.0449</td> </tr> <tr> <td>R-Sq</td> <td>88.9%</td> </tr> <tr> <td>R-Sq(adj)</td> <td>83.3%</td> </tr> </table>	—	Regression	- - -	95% CI	S	15.0449	R-Sq	88.9%	R-Sq(adj)	83.3%
—	Regression										
- - -	95% CI										
S	15.0449										
R-Sq	88.9%										
R-Sq(adj)	83.3%										
<p>Zone II (treated at 1.0 mm depth)</p>	<p style="text-align: center;">Zone 2 - Fitted Line Plot</p> <p style="text-align: center;">Vertical length of crack,um = - 91.54 + 127.6 Laser Power, W</p>  <table border="1" data-bbox="1230 1142 1409 1283"> <tr> <td>—</td> <td>Regression</td> </tr> <tr> <td>- - -</td> <td>95% CI</td> </tr> <tr> <td>S</td> <td>8.25751</td> </tr> <tr> <td>R-Sq</td> <td>94.4%</td> </tr> <tr> <td>R-Sq(adj)</td> <td>93.4%</td> </tr> </table>	—	Regression	- - -	95% CI	S	8.25751	R-Sq	94.4%	R-Sq(adj)	93.4%
—	Regression										
- - -	95% CI										
S	8.25751										
R-Sq	94.4%										
R-Sq(adj)	93.4%										

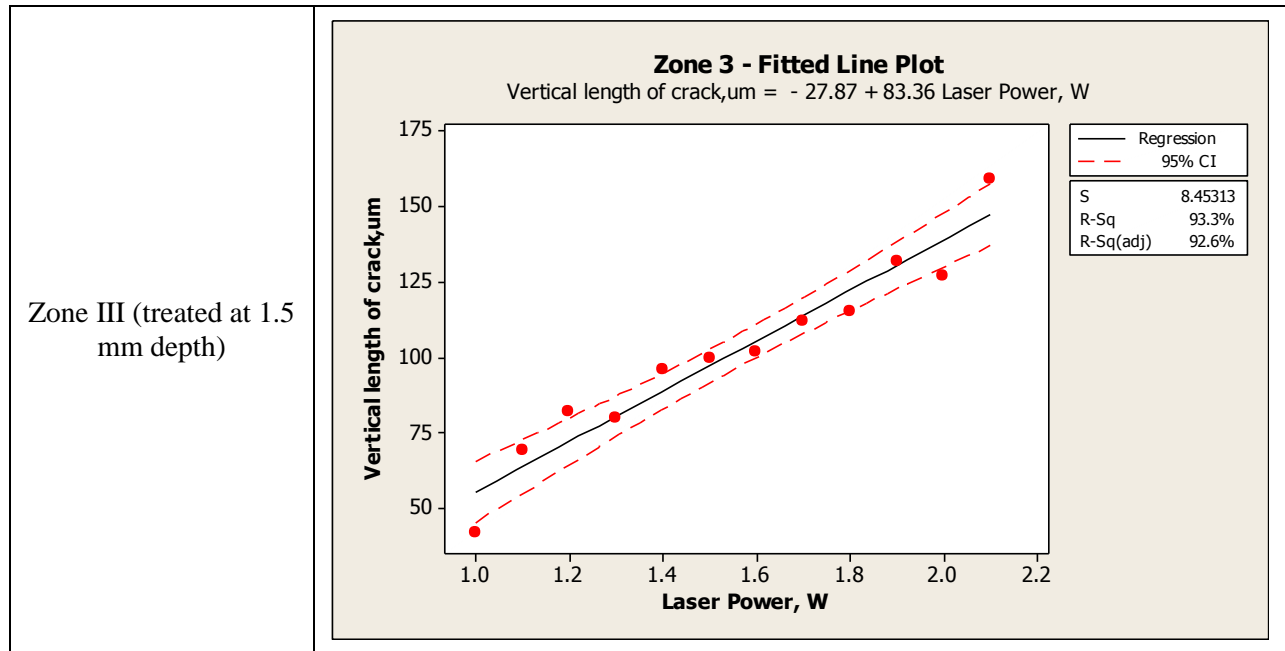


Table 4.5 Optical images of the laser-treated sample from a cross-sectional view with laser beam passing from right to left direction

Description	Laser Cracks (cross-sectional view)- with Labelled Laser Intensities
Zone I (treated at 0.5 mm depth)	

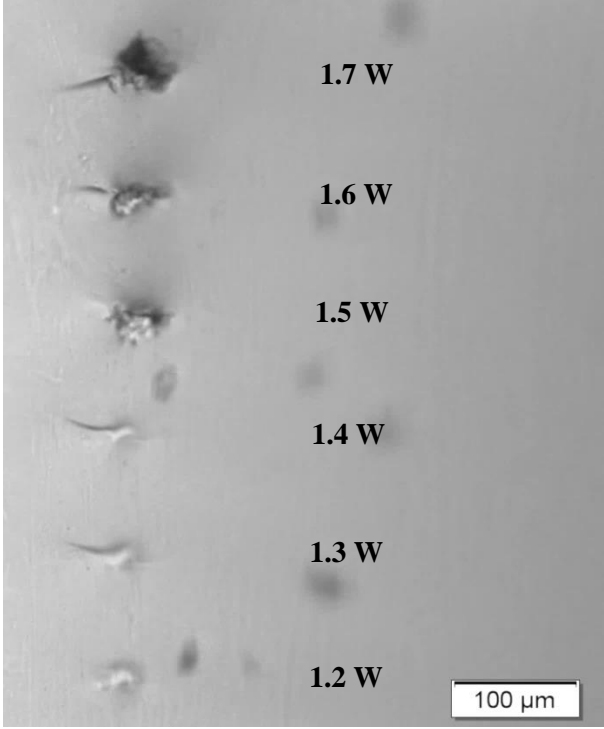
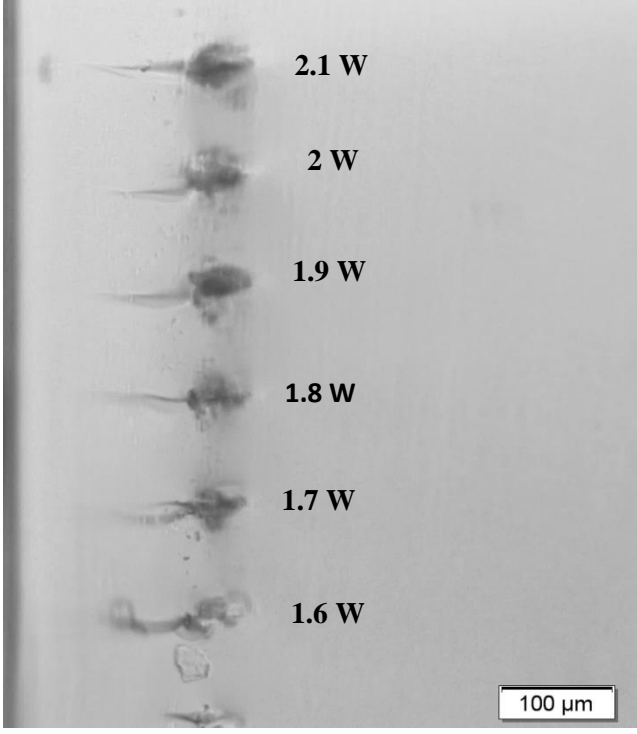
<p>Zone II (treated at 1.0 mm depth)</p>	
<p>Zone III (treated at 1.5 mm depth)</p>	

Table 4.5 illustrates a cross-sectional view of laser cracks induced at different zones for varying laser power. As shown in the table, increased laser power and shallower depth led to increased linear propagation of the crack into the surface. Material depth had higher influence on the crack propagation.

As observed in Zone I image of Table 4.5, linear propagation of the crack increased with the corresponding laser power used to induce it.

In summary, the study on laser treatment in bulk BK7 glass provided a fundamental understanding of the structural and dimensional profile of laser cracks. Variation of crack structure with respect to laser power and material depth was analyzed. Study results showed that the propagation of cracks beyond the intended damage spot is a major concern from an experimental point of view. In this case, there will be presence of subsurface damages or surface cracks due to laser machining upon conventional machining of these treated materials. The cracks propagating beyond the surface would impact adversely on the quality of the final product by reducing the strength and retaining impurities. It can be argued that the focal spot of the crack can be adjusted based on the desired depth of cut and the linear propagation of crack beyond the focal point. But the random nature of crack propagation and inconsistency of its dimension will be a challenge. Moreover the effectiveness of these thin-elongating cracks at the desired depth of cut will be comparatively less than the cracks with its originating focal point at the intended depth of cut.

Based on the results from the preliminary study, it was decided to produce cracks without propagation beyond the desired depth of cut in bulk material. To achieve that, a comparatively lower magnitude of laser power than that of those used in preliminary tests was used to produce grooves through multiple scan runs, starting from the material surface to the intended depth of cut. Each groove on the surface is fabricated by scanning the sample across the laser focus at a speed of 1 mm/s, with a laser power of 300 mW. To increase the groove depth, the scanning is repeated 4 or 8 times for each groove. The distances between grooves are chosen as 0.1 and 0.2 mm. A total of six samples are prepared, and the laser parameters used in the fabrication and the resulting groove dimensions are listed in Table 4.6.

Table 4.6 Groove dimensional profile

Sample	1	2	3	4	5	6
Laser power (mW)	300					
Number of scanning (times)	4	4	4	8	8	8
Distance between each groove (mm),D	0.1	0.15	0.2	0.1	0.15	0.2
Average groove width (mm), w	0.063	0.063	0.063	0.070	0.070	0.070
Average groove depth(mm), d	0.1	0.1	0.1	0.2	0.2	0.2

4.4 Results and Discussion

After laser micromachining, the samples are cleaned using an ultrasonic cleaning process. Each sample individually is immersed into the beaker containing distilled water and placed inside an ultrasonic cleaner bath filled with tap water. Sonic vibration process is initiated for 2-3 minutes after which the sample is removed from the ultrasonic bath. After ultrasonic cleaning, the machined samples are carefully wiped with ethanol to remove the glass debris and are allowed to dry. All the four samples are observed under optical microscope before and after cleaning to make sure that no cracks are created during the cleaning process. The damage profile under each machining condition is measured and recorded. Figure 4.6 shows the crack profile nomenclature.

Crack Profile Nomenclature:

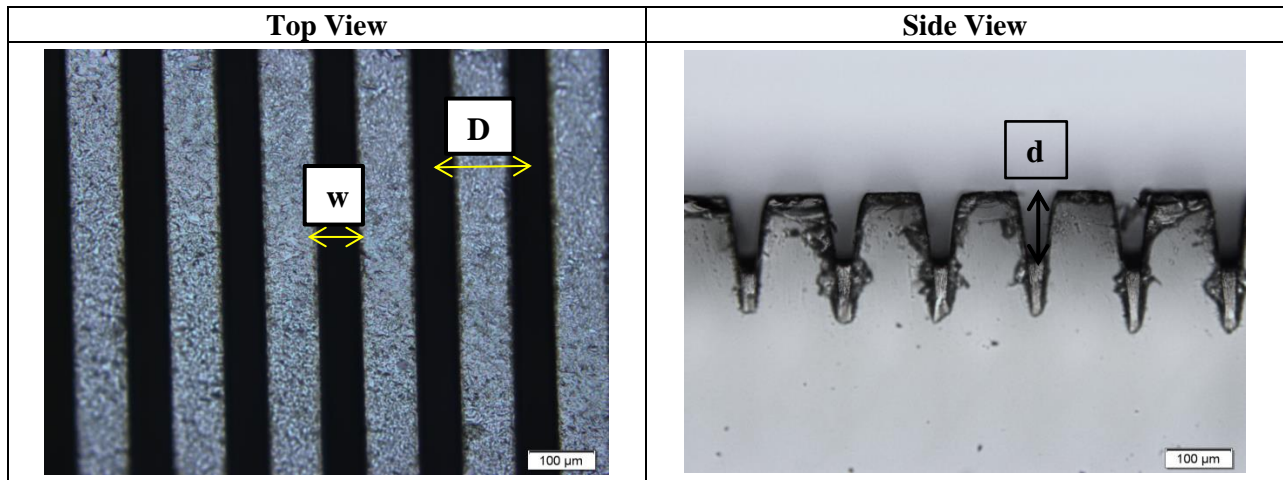
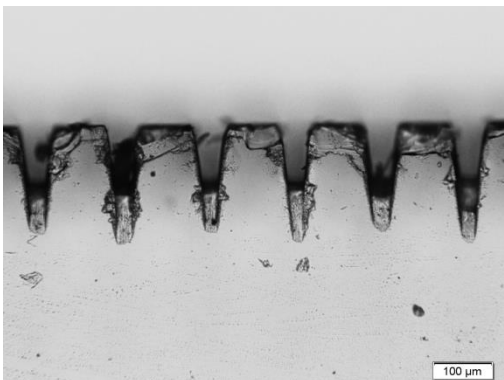
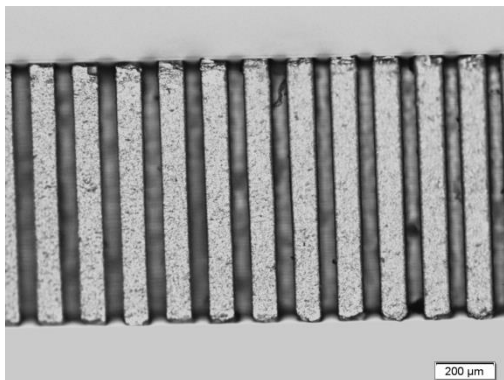
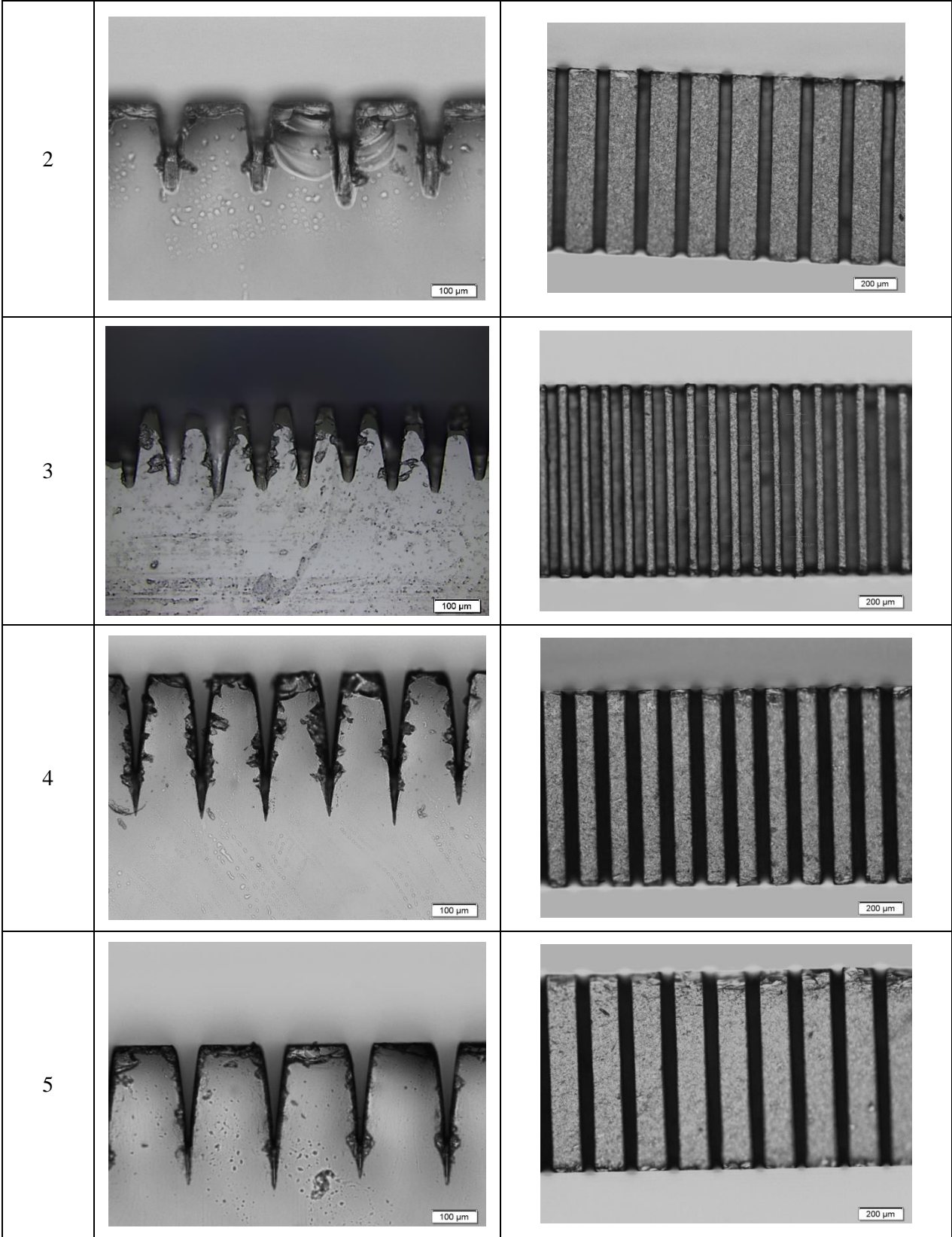


Figure 4.6 Crack profile nomenclature

Table 4.7 Optical images of laser cracks

Sample no	Side View	Top View
1		



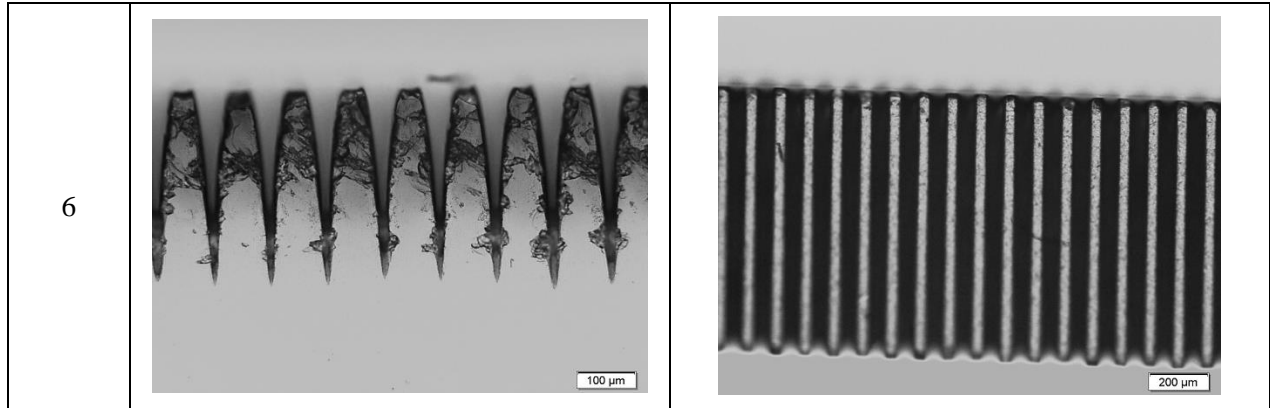


Table 4.7 shows optical images of the laser cracks for all six laser machined samples. For each sample, multiple images were taken using an optical microscope and measurements were made for the groove depth, groove width and the distance between each groove from 10 to 15 observations for each sample in order to determine the average value. Damage to material walls was also measured and an average surface area of wall damage for a groove on each of the six samples was calculated.

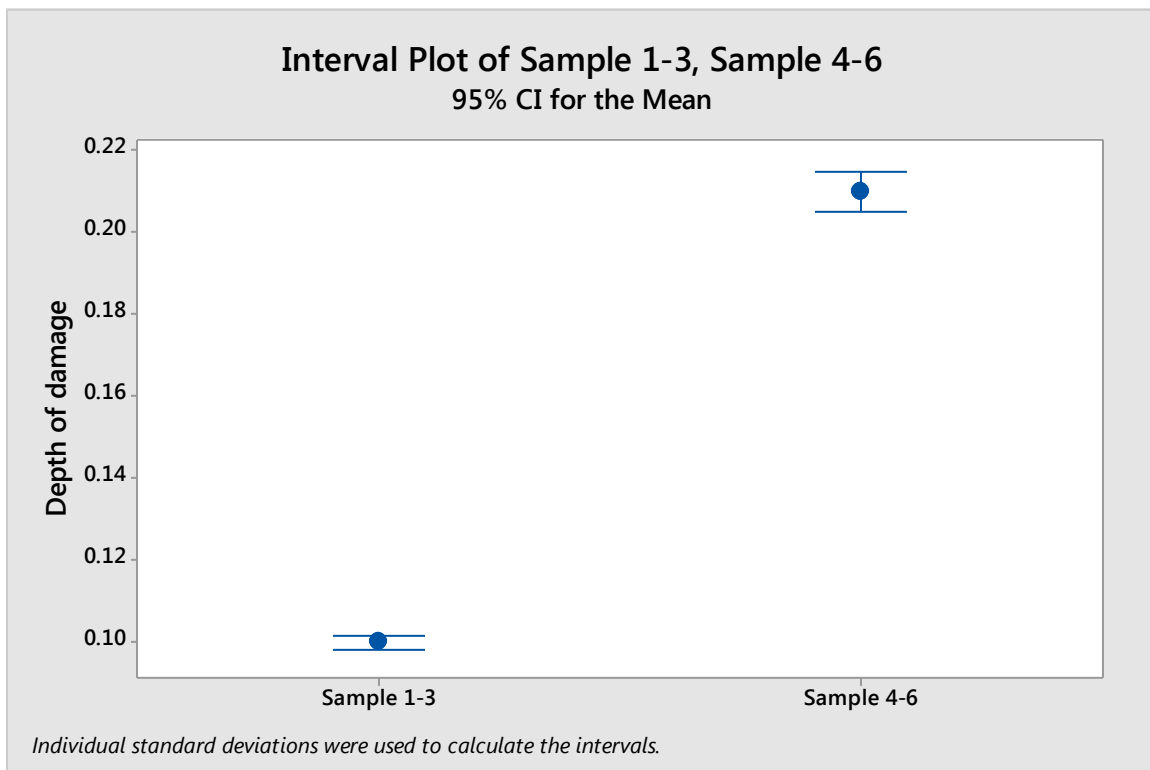


Figure 4.7 Interval plot for groove depth measurement

Figure 4.7 shows, groove depth of all six samples measured and plotted in an interval plot using Minitab 17 statistical tool. Samples 1, 2, and 3 had an average groove depth of approximately 0.1 mm. Samples 4

,5, and 6 have an average groove depth of 0.21mm. Measurement of groove depth was done to ensure that the damage did not propagate beyond the predetermined experimental depth of groove.

However, micro-cracks and damages were noted on the side walls of the grooves in all samples as shown in Figure 4.8. The surface area of the damage on a set of individual grooves was measured in all samples.

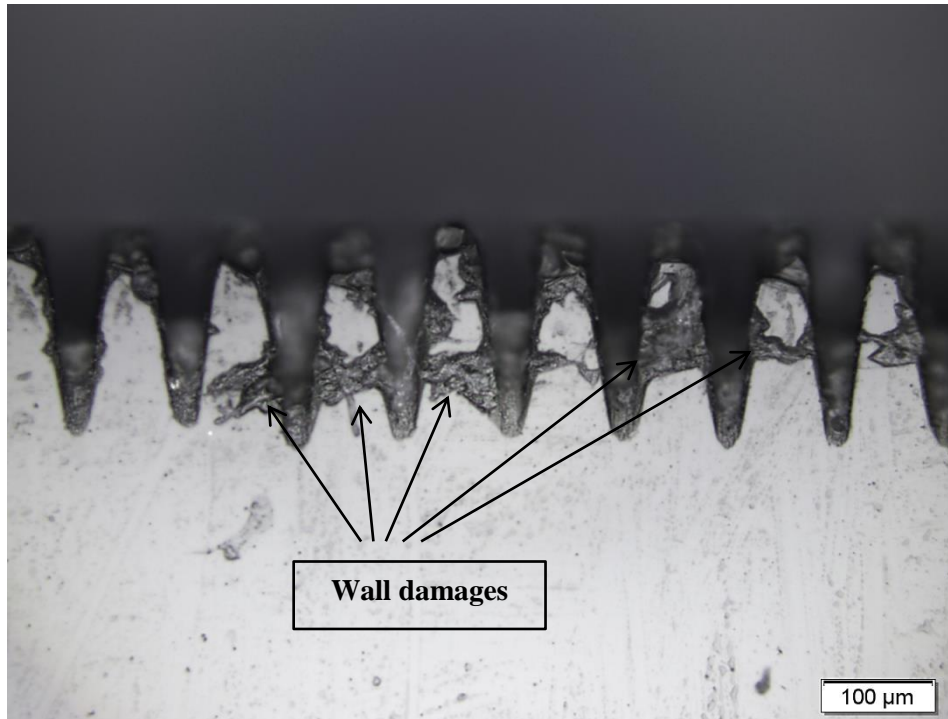


Figure 4.8 Groove wall damages from side view of Sample 2.

Table 4.8 Wall damage measurement

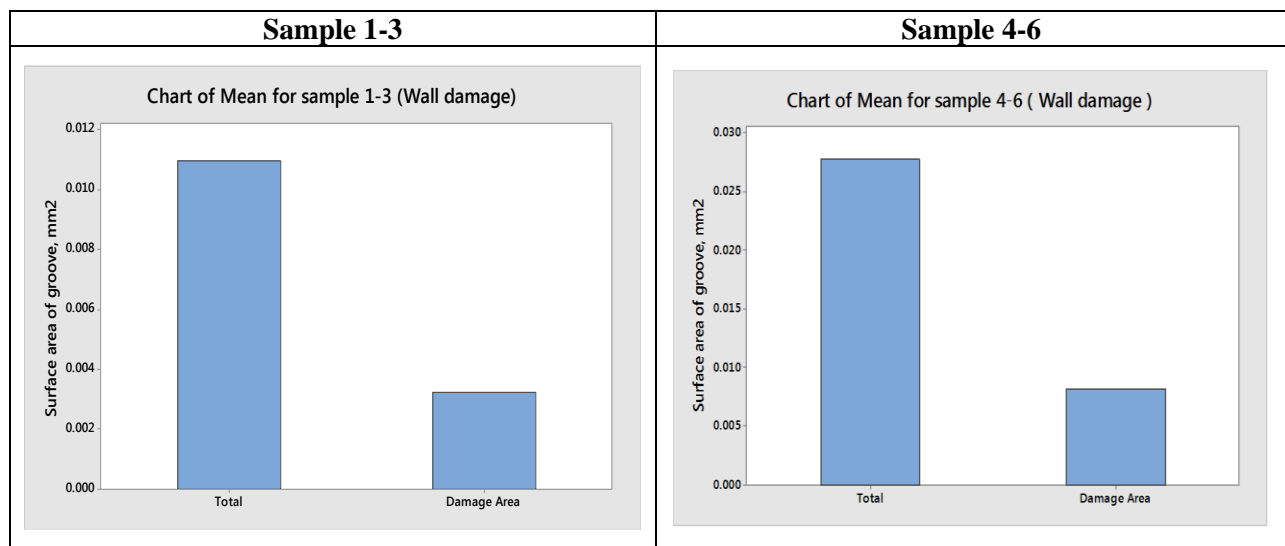


Table 4.8 shows, the measured average surface area of individual groove from all samples, plotted as total in a bar chart using Minitab 17 statistical tool. The damaged area on an individual groove from all samples was also plotted. Approximately 33% of the total groove surface area was damaged. For Samples 1-3, the average surface area of an individual groove was 0.011 mm^2 , and on average 0.003 mm^2 of the surface area was damaged. Similarly for Samples 4-6, the average surface area of an individual groove was approximately 0.027 mm^2 , and on average 0.008 mm^2 of the surface area showed damage. These damages were attributed primarily to an expanded heat-affected zone, material evaporation and thermal stress developed during laser micromachining.

After analyzing groove geometry, the average depth of groove was fixed as the depth of cut for orthogonal machining. In his experiments, two average groove depths (0.1 mm and 0.2 mm) of laser micromachined samples were taken as the depth of cut for machining.

Chapter 5 Orthogonal Machining

5.1 Background

Orthogonal machining or (2D machining) neglects many geometric complexities found in other machining processes, such as turning, milling and drilling. Orthogonal machining uses a single point cutting tool with a cutting edge that is perpendicular to the cutting direction. Figure 5.1 illustrates the orthogonal machining process. As the tool comes into contact with the material, the cutting chip is formed by shear deformation along the shear plane oriented at an angle with the surface of the work piece. At the cutting zone either plastic deformation (for ductile materials) or fracture (for brittle materials) occurs. The rake angle denotes the angle of the cutting face relative to the work sample and determines the direction of chip flow as it is formed. The clearance angle provides a small clearance between tool flank and newly generated work surface.

The primary reason for choosing orthogonal machining for this research was that the fundamentals of the cutting process are often best understood through studies that employ simple tool geometry and process kinematics as offered by the orthogonal cutting process. With knowledge gained from orthogonal machining, extensions to other commonly used machining processes, such as milling and turning is natural progression [40].

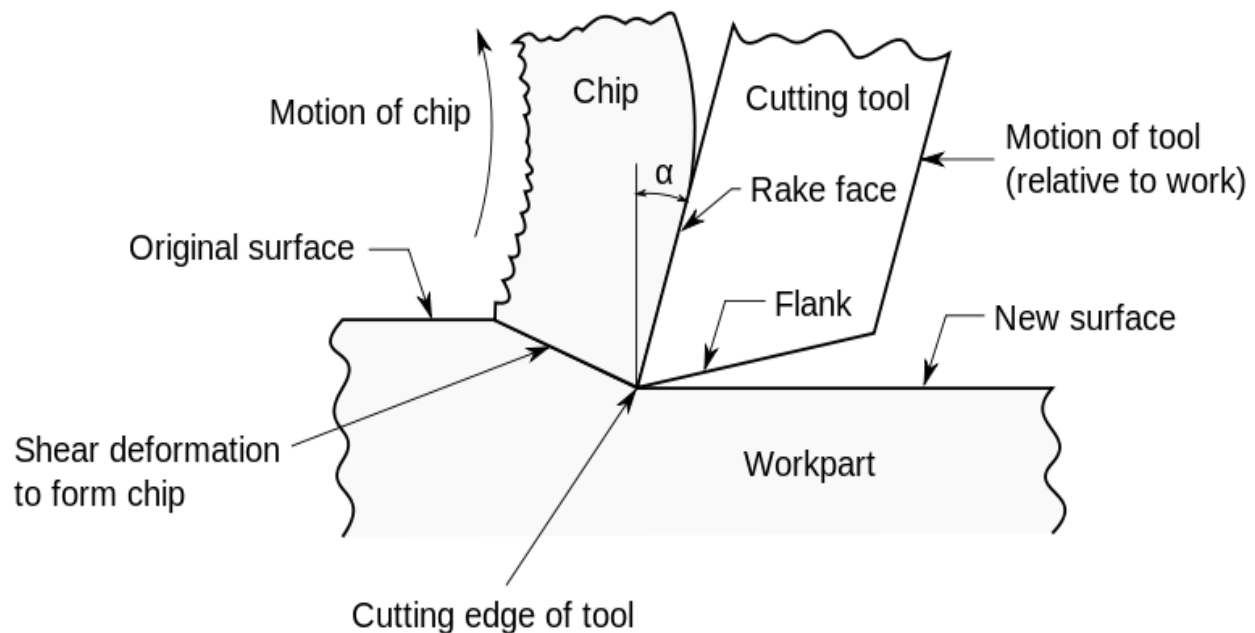


Figure 5.1 Schematic of the orthogonal machining process [40]

5.2 Experimental Setup

The orthogonal machining experiment was setup using a vertical Bridgeport milling machine with the cutting tool fixed to the locked vertical spindle column. The workpiece was fixed to a horizontal movable carriage, as shown in Figure 5.2.

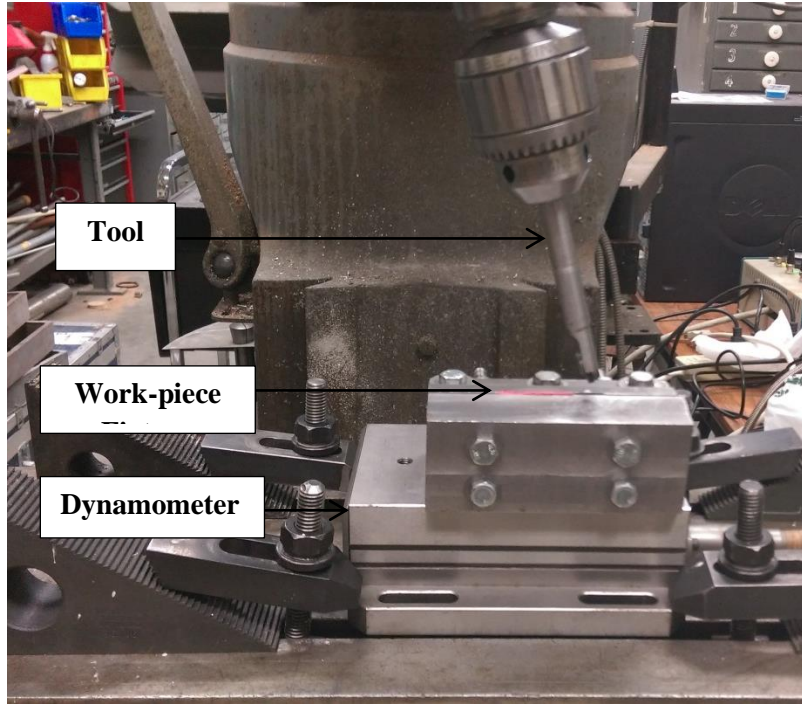


Figure 5.2 Experimental setup of the orthogonal machining process

The workpiece – fixture component was mounted onto a Kistler three-component dynamometer. A Kistler dual-mode charge amplifier was used to amplify signals of cutting forces measured by the dynamometer. The computer data acquisition system was controlled by LabVIEW. The workpiece, fixture, and dynamometer, were clamped onto the movable carriage of the Bridgeport milling machine. The horizontal carriage fed the workpiece on to the stationary tool holder mounted in the vertical tool chuck.

Table 5.1 Machining parameters

Machining Conditions	
Cutting speed (mm/second)	4.23
Depth of Cut (mm)	0.1,0.2
Length of cut (mm)	25.4

Work piece: Borosilicate glass schott samples (BK7) measuring 25.4 mm square and 1mm thick were used as workpieces for the experiments. BK7 glass is the most commonly used high-quality optical glass;

it offers good optical properties and high resistance to chemical attack and no special handling is required, which reduces its manufacturing cost. Most windows, lens, and prisms used in laser, optical system, and optical communication are made from BK-7 glass. Due to its highly homogenous and clean microstructure, BK-7 glass is extremely suitable for manufacturing a wide range of products such as injection molds for plastic products [41]. Therefore, the machinability of BK7 glass must be improved in order to achieve minimal or defect-free surfaces, which will increase the expected fatigue life of glass mold in case of injection mold manufacturing applications.

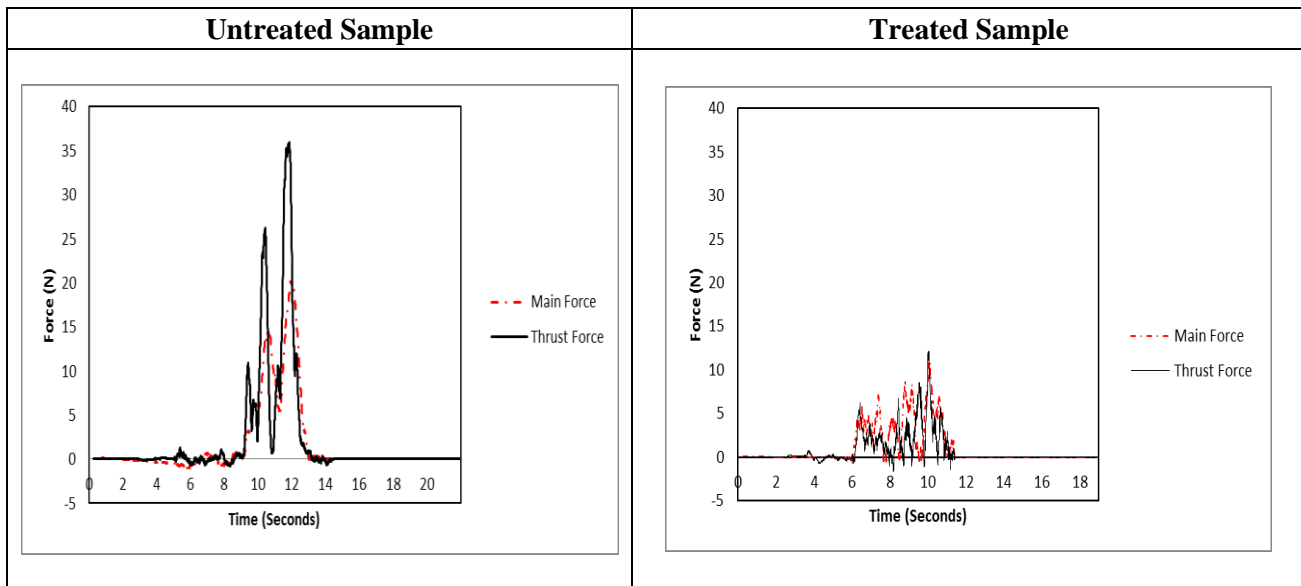
Cutting tool: A 5.5mm square shaped cubic boron nitride (CBN) was used as a cutting tool insert .A special tool holder, tilted to attain a negative 15 degree rake angle is used for the experiment.

Chip samples: Cutting chips were collected during the experiments. The chips were ejected in all directions during cutting, so the flying chips were collected using plastic bags that enclosed the work fixture during machining. Chip fragments were examined using an optical microscope.

5.3 Results and Discussion

5.3.1 Comparison of Cutting Force

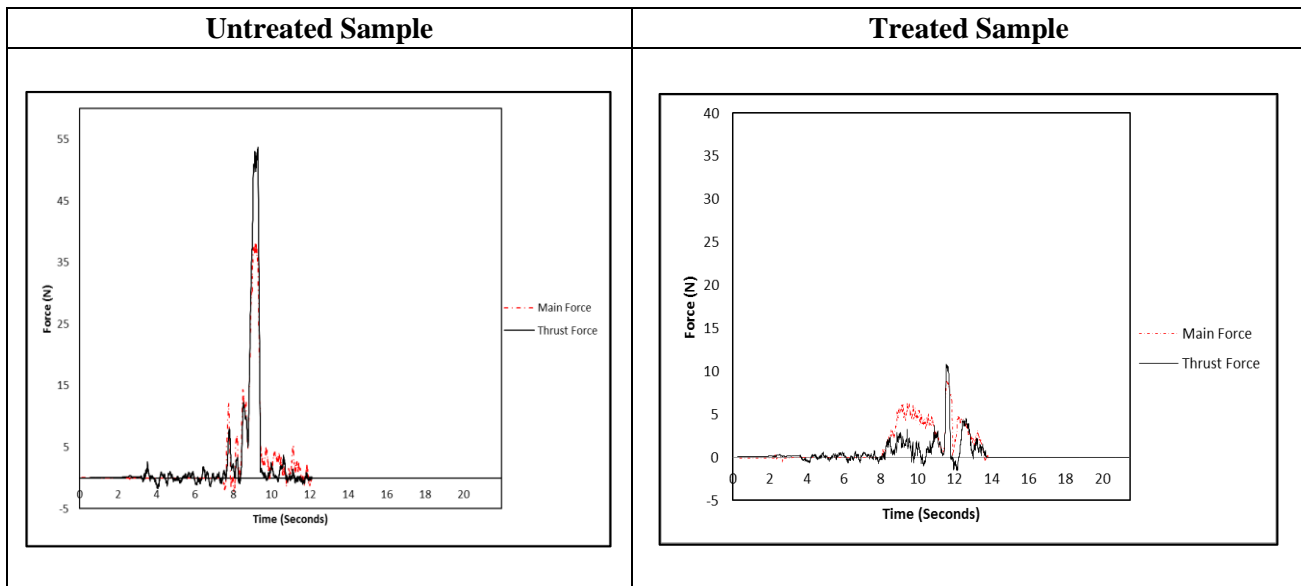
Table 5.2 comparison of forces (depth of cut: 0.1 mm; feed rate: 4.23 mm/s)



Three rounds of machining experiments , each with depth of cut of 0.1 mm and 0.2 mm, are performed on the untreated samples and the average force components were plotted against the cutting time. The cutting force in orthogonal machining has two components – thrust force: perpendicular to the direction of cut and main force: acting along the direction of cut. Before conducting machining experiments, the dynamometer was calibrated. Force data was plotted in Microsoft Excel at a sampling rate of 200 data

points per second. Force components were plotted using a moving average trend line with a single point in the graph formed by averaging 25 data points from raw data. Machining experiments on treated samples were repeated thrice on each with depth of cut of 0.1 mm and depth of cut of 0.2 mm. It can be seen clearly from Table 5.2 that there is a significant reduction of cutting force on machining treated samples. The peak force and average cutting force for the untreated BK7 sample machined at depth of cut of 0.1 mm and feed rate of 4.23 mm/s were 35 N and 15 N, respectively, for the thrust force and 20 N and 12 N, respectively, for the main force. While the peak force and the average cutting force for the laser treated sample for the same conditions were 12 N and 3 N, respectively, for the thrust force and 10 N and 4 N, respectively, for the main force. The reduction was 65% in peak thrust force, 67% in average thrust force, 50% in peak main force and 43% in average main force.

Table 5.3 Comparison of forces (depth of cut: 0.2 mm, feed rate: 4.23 mm/s)



Similarly, when machining with depth of cut of 0.2 mm, a notable reduction in cutting force of the treated sample (Table 5.3) was observed. Machining of the untreated sample revealed peak values of 54 N and 39 N for the thrust and main cutting force, respectively. Machining of the treated sample yielded peak values of 11 N and 9 N for the thrust and main cutting force respectively. Comparatively, a reduction of 79% and 77% in the peak thrust and main cutting force respectively occurred for the treated samples. The average thrust and main cutting force, for the treated sample showed 80% and 66% force reduction, respectively.

5.3.2 Design of Experiments

Comparative balanced experimental designs with three replications were performed for the orthogonal machining experiments. Two set of experiments were completed. Experiment I was done with a depth of

cut of 0.1 mm and Experiment II was done with a depth of cut of 0.2 mm. Each set of experiment is repeated three times under the same conditions, and the average cutting forces were recorded as shown in Table 5.4.

Table 5.4 Average cutting force for each trial of experiments

Experiment	Replications	Average Force (N)			
		Untreated		Treated	
		Thrust force	Main force	Thrust force	Main force
I	1	17.785	14.180	2.029	3.124
	2	15.031	12.552	2.925	4.047
	3	16.728	14.041	2.689	3.215
II	1	19.968	15.506	4.381	5.629
	2	18.163	14.654	4.685	6.496
	3	19.245	14.859	3.985	5.462

Analysis of variance(ANOVA) was performed to statistically establish that the average cutting force between two models (untreated and laser treated) differed significantly. Figure 5.3 shows the cumulative average cutting force with standard error bars.

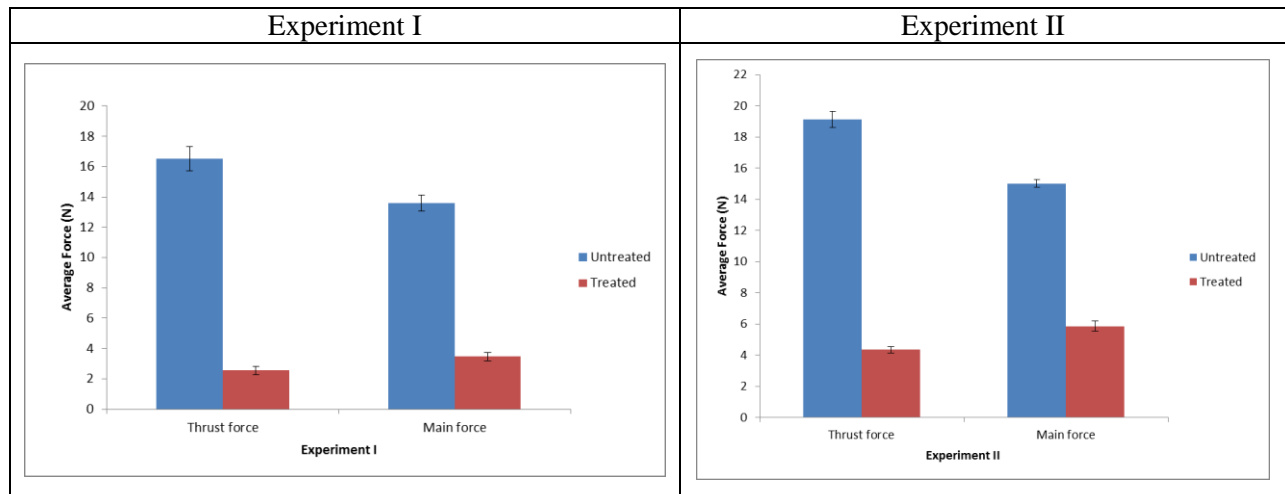


Figure 5.3 Average cutting force with standard error bars

ANOVA clearly showed a highly significant *p*-value for both types of experiments and therefore, the null hypothesis was rejected and concluded upon the evidence for mean cutting force differences between the treated and untreated samples at 5% level of significance. The following one way ANOVA tests were performed using a Minitab 17.

One-way ANOVA: Experiment I

Null hypothesis All means are equal
Alternative hypothesis At least one mean is different
Significance level $\alpha = 0.05$

Equal variances were assumed for the analysis.

Factor Information

Factor	Levels	Values
C1	2	treated, Untreated

Analysis of Variance

Source	DF	Adj SS	Adj MS	F-Value	P-Value
C1	1	435.46	435.463	212.28	0.000
Error	10	20.51	2.051		
Total	11	455.98			

Model Summary

S	R-sq	R-sq(adj)	R-sq(pred)
1.43227	95.50%	95.05%	93.52%

Means

C1	N	Mean	StDev	95% CI
treated	6	3.005	0.664	(1.702, 4.308)
Untreated	6	15.053	1.914	(13.750, 16.356)

Pooled StDev = 1.43227

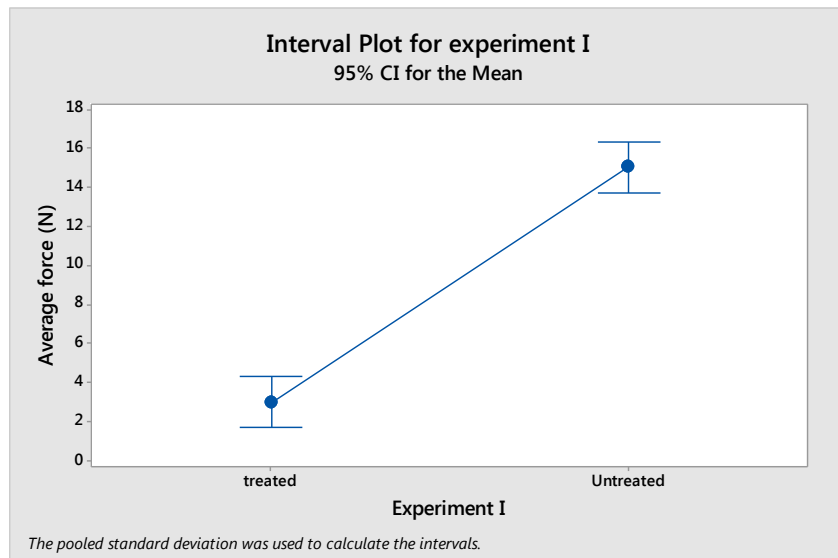


Figure 5.4 Interval plot for average cutting forces for Experiment I

One-way ANOVA: Experiment II

Null hypothesis All means are equal
Alternative hypothesis At least one mean is different
Significance level $\alpha = 0.05$

Equal variances were assumed for the analysis.

Factor Information

Factor	Levels	Values
C1	2	treated, Untreated

Analysis of Variance

Source	DF	Adj SS	Adj MS	F-Value	P-Value
C1	1	429.09	429.089	134.99	0.000
Error	10	31.79	3.179		
Total	11	460.88			

Model Summary

S	R-sq	R-sq(adj)	R-sq(pred)
1.78289	93.10%	92.41%	90.07%

Means

C1	N	Mean	StDev	95% CI
treated	6	5.106	0.926	(3.485, 6.728)
Untreated	6	17.066	2.345	(15.444, 18.688)

Pooled StDev = 1.78289

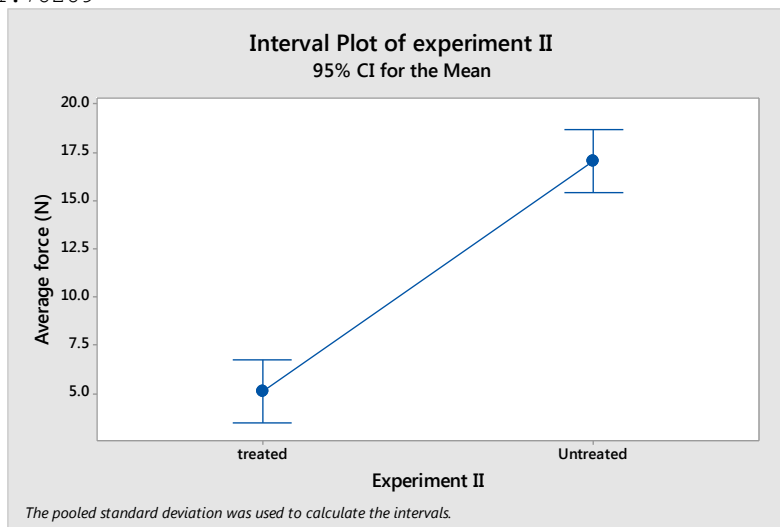


Figure 5.5 Interval plot for average cutting forces for Experiment II

5.3.3 Surface Integrity: Untreated Sample

After machining, the samples were examined for surface and subsurface cracks using an optical microscope. In order to assess SSDs in the untreated machined sample, the subsurface were classified into three zones as given in Table 5.5.

Table 5.5 Zone Classification for SSD

Zone	Depth range from the top machined surface, mm
I	0.2-0.4
II	0.4-0.7
III	0.7-0.9

For example, any crack or damage below 0.2 mm from the top machined surface comprised Zone I. If the damage area propagated beyond a depth of 0.4 mm, it was classified under Zone II. Beyond 0.7 mm depth, it was classified Zone III. Two parameters were measured and recorded: - (1.-) linear dimension of the crack or the length of the damage propagating below the machined surface, D ; and (2.-) Surface area affected by the crack in the respective zone, A . Figure 5.6 illustrates zone classification.

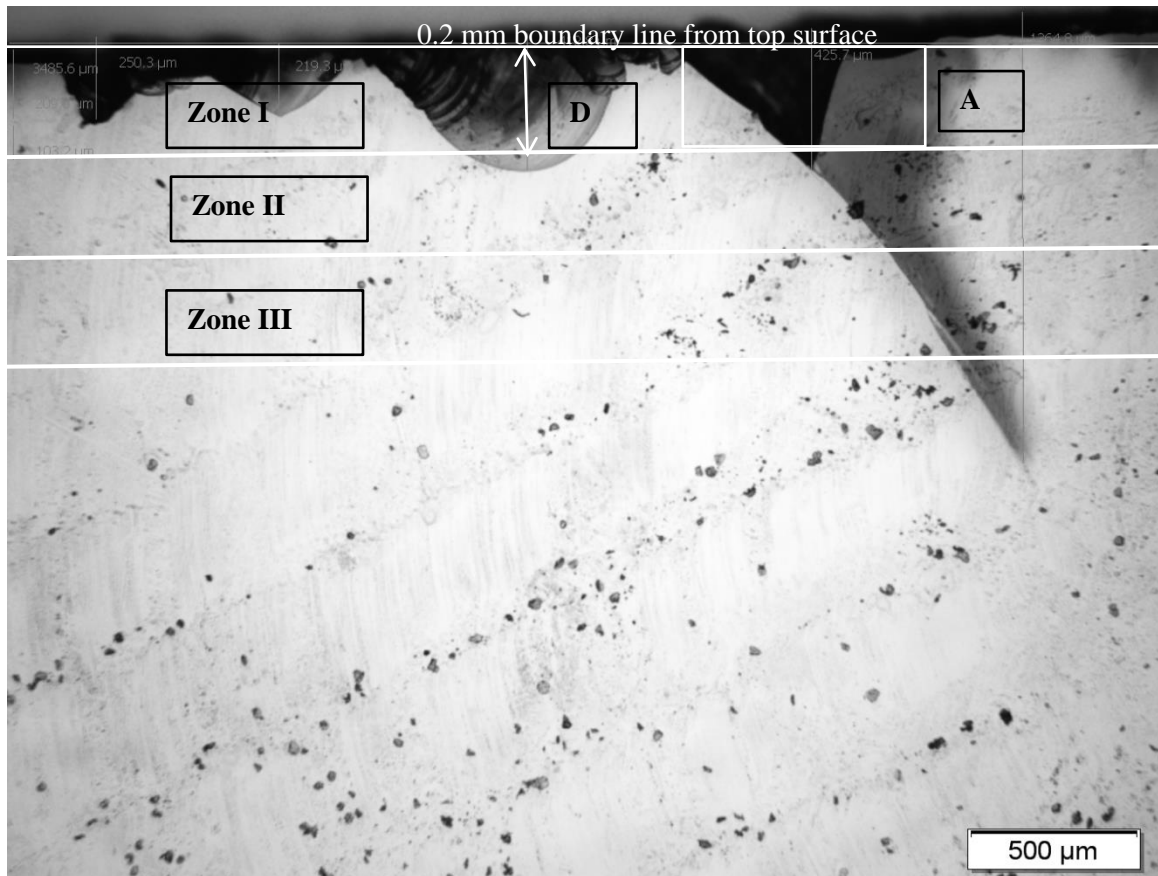
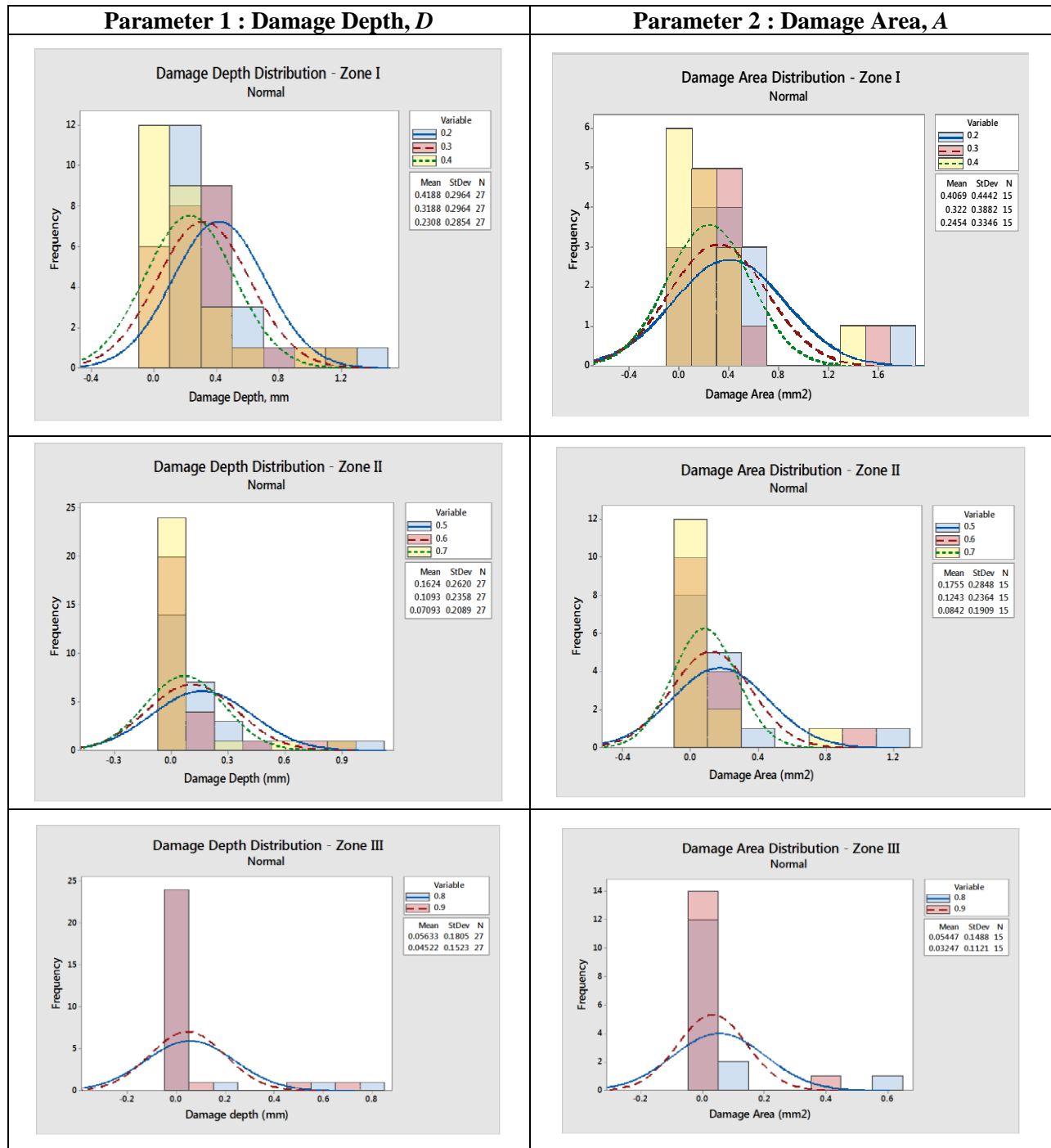


Figure 5.6 Zone classification and nomenclature

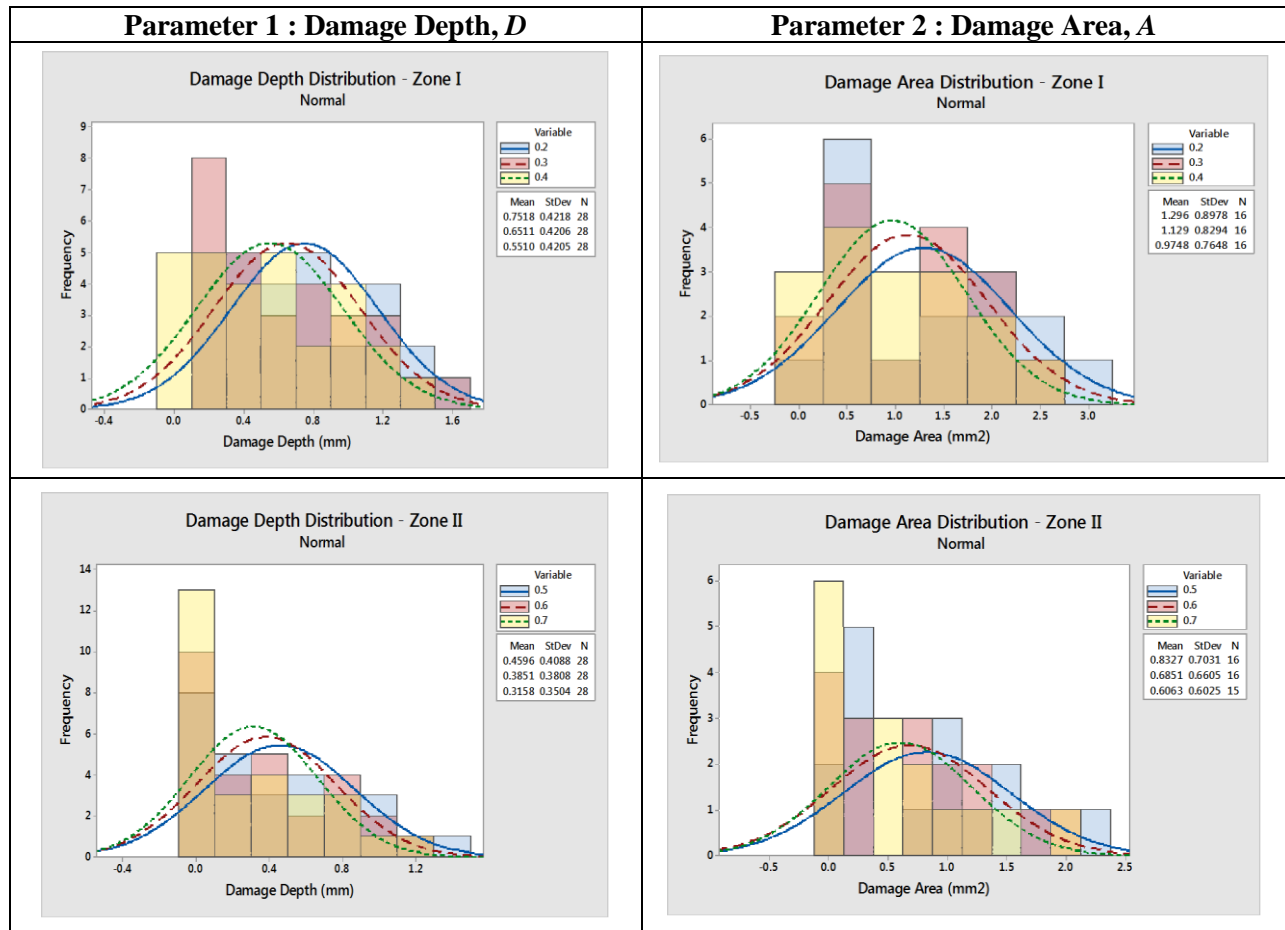
Table 5.6 Damage distribution chart for untreated samples: depth of cut: 0.1 mm



Conventional machining of BK7 glass produces surface distortion and subsurface cracks due to its hard and brittle nature. In Table 5.6, cracks are classified based on their propagation beyond the machined surface after machining an untreated sample at a depth of cut of 0.1 mm. After machining untreated samples, the subsurface cracks of each sample were measured and classified into respective zones. Classified SSDs were plotted in a histogram using Minitab 17. The histogram showed the damage depth

and damage area distribution for all three zones. Results showed that the cracks decreased in size and area as the depth increases. For example at 0.2 mm below the machined surface, the cracks propagated an additional 0.418 mm on average into the workpiece. While at 0.3 mm below the machined surface, average crack propagation was 0.318 mm in bulk sample. Such classification of subsurface cracks helps further in understanding of the distribution and frequency of crack propagation upon machining. Because cracks propagate in all directions, average area distributions of damage at various depths were also determined. In Zone II, below the 0.5 mm depth, damages had an average size of 0.175 mm^2 , measuring 0.124 mm^2 on average at a depth of 0.6 mm. Because Zone III was comprised of depth greater than 0.7 mm, crack propagation beyond this level was minimal, at an average of 0.05 mm.

Table 5.7 Damage distribution chart for untreated Machining Test II: depth of cut: 0.2 mm



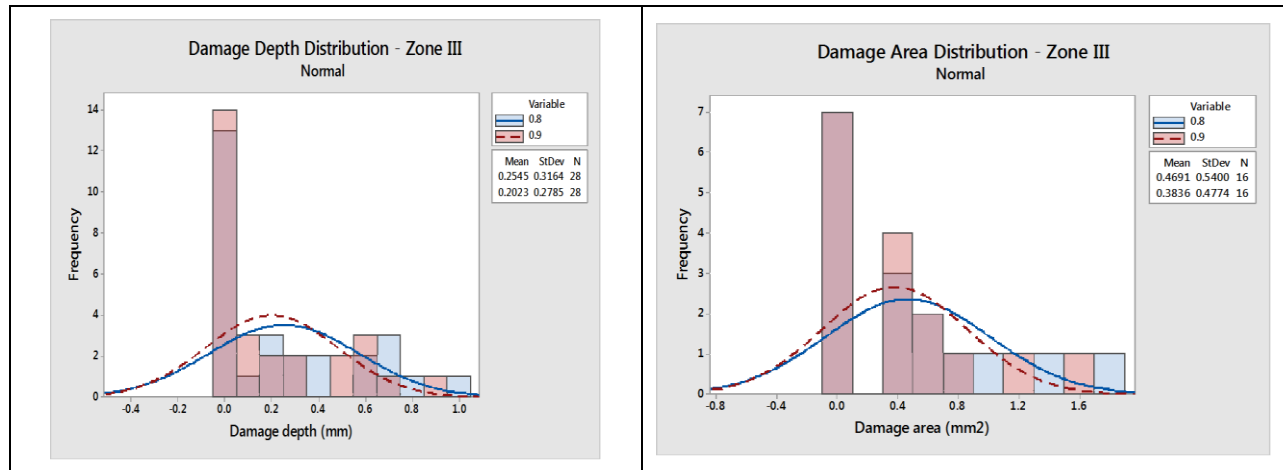


Table 5.7 summarizes damage distribution resulting from machining experiments with depth of cut at 0.2 mm. Results showed that damage depth and area increased as depth of cut increased. The main objective behind the usage of a histogram was to understand damage propagation and the distribution of cracks based on depth and other machining conditions. Determination and comparison of SSD between various machining conditions assists process improvement leading to better material quality. Reduction of SSDs is considered as a very important factor for improving material quality. Table 5.6 shows an increase in SSD propagation with an increase in depth of cut. For instance, the average damage depth that propagate beyond the 0.2 mm level with 0.1 mm depth of cut was 0.418 mm, while it was 0.751 mm for the 0.2 mm depth of cut. Similarly the damage surface area also increases with depth of cut. Therefore, with higher material removal rate, the surface integrity worsened and cracks propagated deeper into the work samples. In all three zones, more subsurface crack propagation was evident compared to machining Experiment I.

Treated Sample:

When the machined surface of the treated samples was investigated using an optical microscope, no or very negligible subsurface cracks were observed. The absence of subsurface damages upon machining laser treated samples will bring a significant improvement in material quality. As discussed in the previous section, the untreated machined samples had a SSDs reaching as far as 2 mm depth. Avoiding SSD is one of the most important results achieved through laser treatment of BK7 glass samples. After analyzing the subsurface damages, the machined surface integrity of both treated and untreated samples was compared. Analysis and comparison of the machined surface helps further understanding of the machining process and chip removal mechanism. A machined surface without major cracks or fracture is an important factor for improving product quality and life span.

Table 5.8 Comparison of machined surface –side view; depth of cut: 0.1 mm

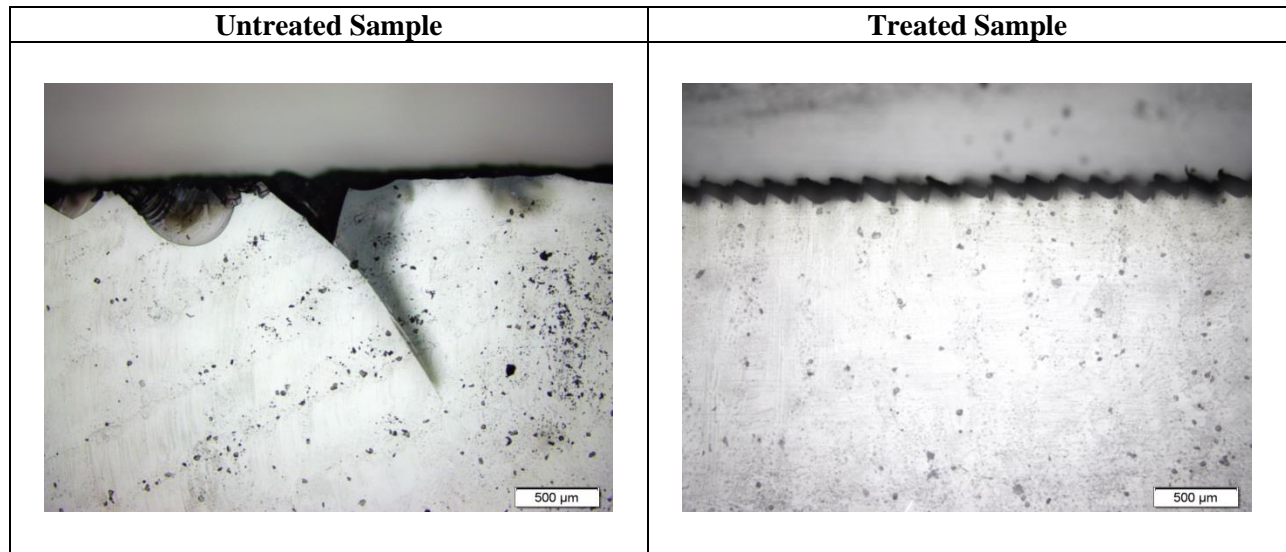


Table 5.8 shows a comparison of the machined surface of the untreated and treated sample machined with depth of cut of 0.1 mm. With the exception of surface modifications due to laser treatment, there are no cracks or SSDs formed due to orthogonal machining.

Table 5.9 Comparison of machined surface –side view; depth of cut: 0.2 mm

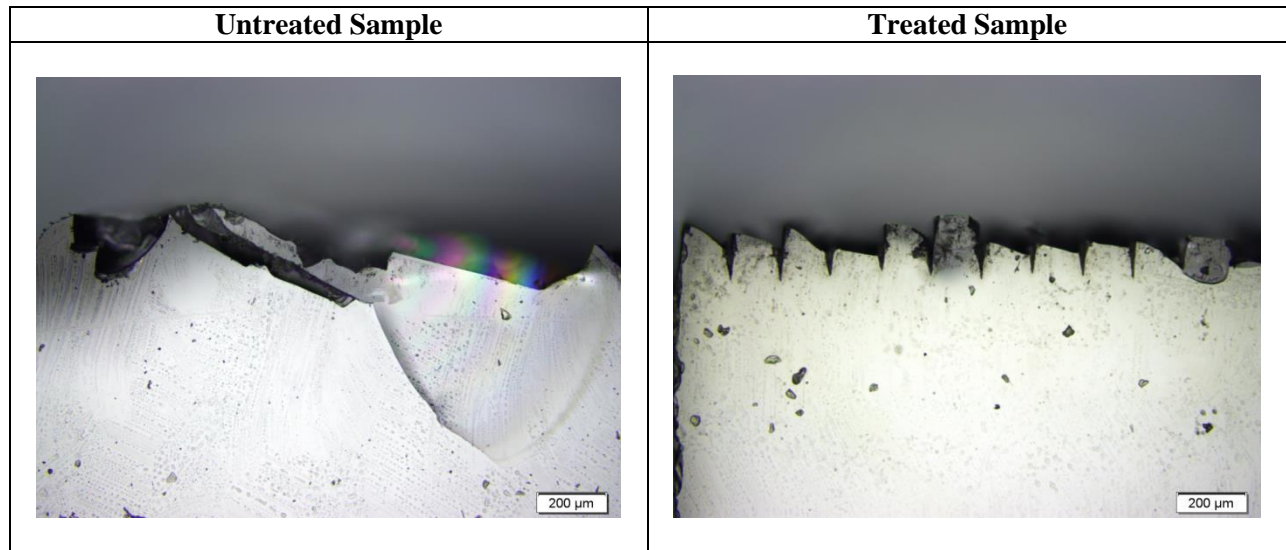


Table 5.9 shows optical images of a machined surface from a side view. As shown the untreated sample developed large cracks upon machining. Cracks shown on the treated sample were wall damages developed during the laser micromachining process but there are no subsurface cracks developed due to

orthogonal machining. Cracks created due to laser machining were comparatively larger for the 0.2 mm groove depth.

Table 5.10 Comparison of machined surface –top view; depth of cut: 0.1 mm

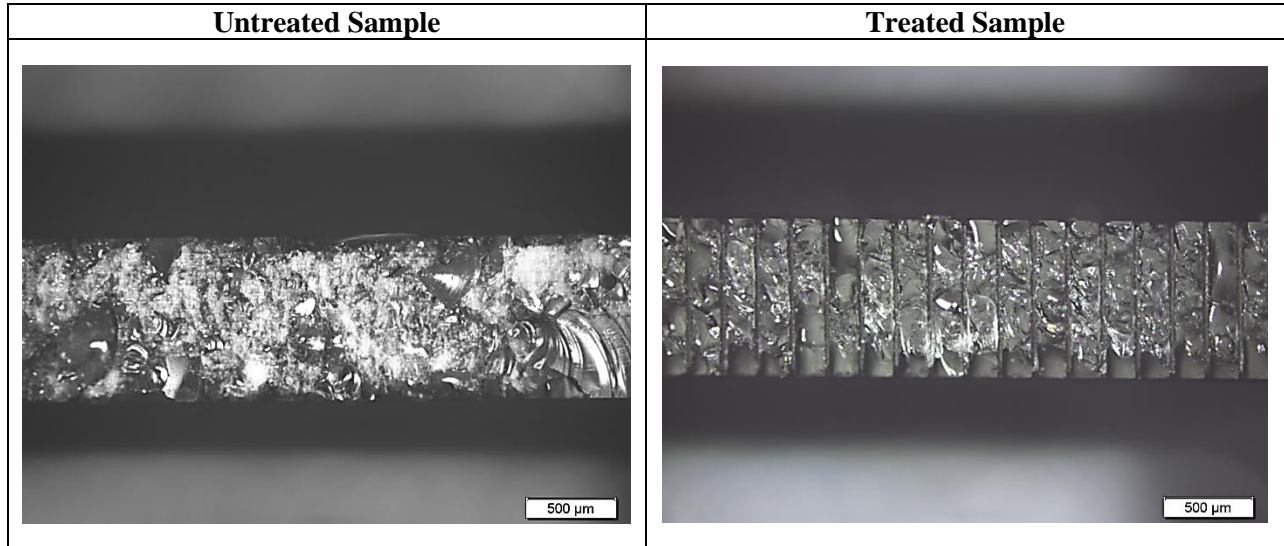


Table 5.10 shows a comparison of a machined surface from top view. Visually analyzing the machined surface helps in determining the material removal mechanism. In the untreated sample, material removal produces chips largely in two forms: powdered chips – (i.e.-very fine particles of chips in forms of powder, obtained as cutting chips, and large chips – (i.e. -comparatively larger chunks of material removed forming a glassy surface on the machined surface).

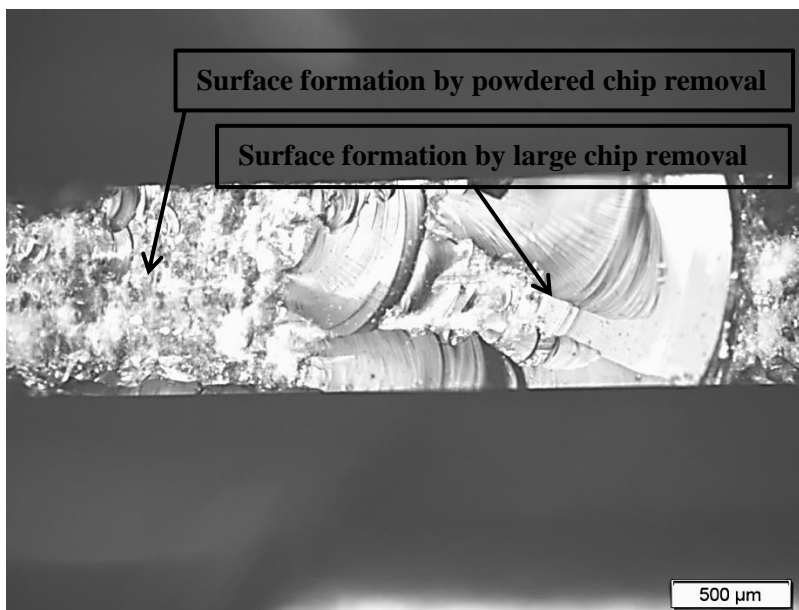


Figure 5.7 Material removal in untreated sample-top view; depth of cut: 0.1 mm

Figure 5.7 illustrates surface formation due to material removal in untreated samples. Material removal in large chunks correlates with high cutting force since high force is required to remove greater amount of material. Removal of large material chips typically distorts the material surface, leading to poor product quality. For treated samples, machined surface exhibited traces of powdered chip removal and clear surfaces inferring material removal in the form of grooves.

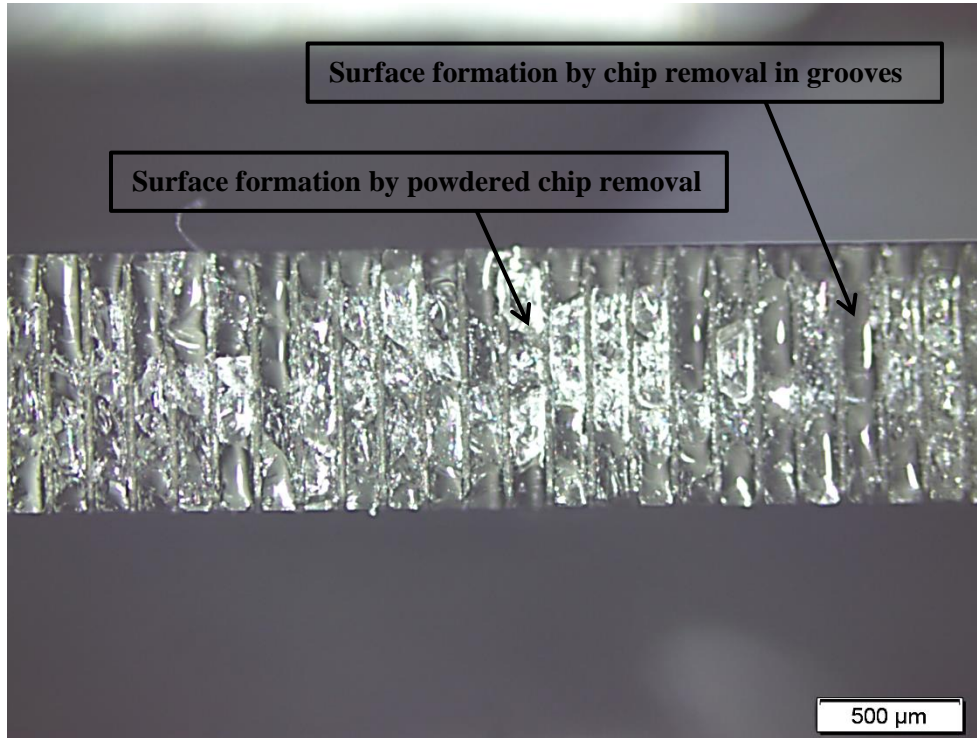


Figure 5.8 Material removal in treated sample-top view; depth of cut: 0.1 mm

Figure 5.8 illustrates surface formation due to material removal in treated samples. Laser machined grooves helped prevent material removal in the form of large chips, resulting in improved surface quality. Material removal through large chips occurred more often with increased material removal rate. For machining of an untreated sample at 0.2 mm depth of cut, material removal showed a comparative increase in form of large chunk of chips resulting in higher surface distortion.

Figure 5.9 shows that, the machined surface area of the untreated sample was classified into surface formation by powdered chips and large chips. As shown, in Machine Test I with depth of cut of 0.1 mm powdered chip formation covered 70% of the machined surface area whereas large chips formed in the remaining 30% of the surface. For Machine Test II with depth of cut of 0.2 mm the powdered chip formation decreased to 30% and the remaining surface formation occurred due to large chip removal.

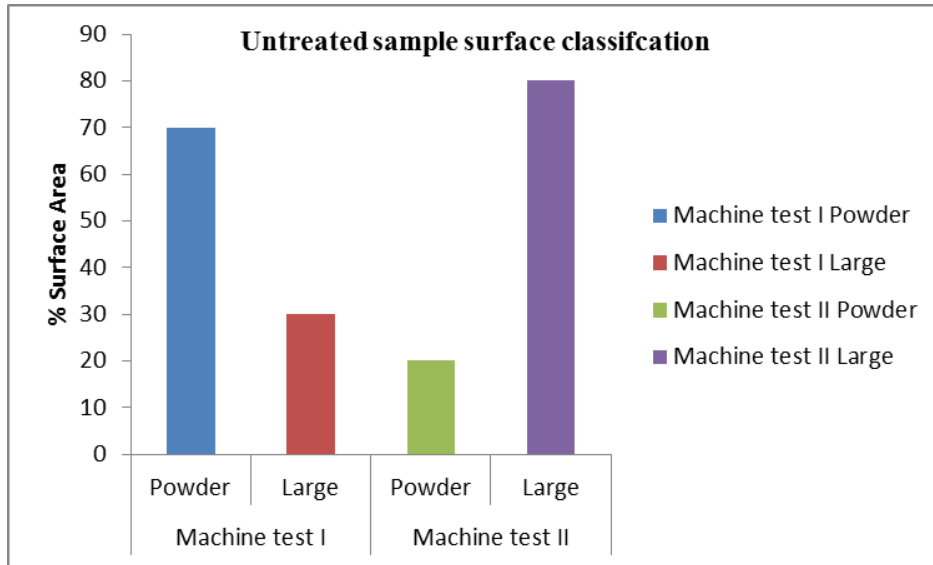


Figure 5.9 Material removal in untreated sample: surface classification

For treated sample, surface formation occurred due to removal of a laser machined grooves in more than 80% of the times in both types of machine tests.

5.3.4 Chip Morphology

As discussed in the experimental setup, flying chips during the machining process were carefully collected in a plastic bag. Each cut generated a range of chip fragments from powder-like to relatively large pieces. Collected chip samples during the machining of laser treated and untreated samples were examined using an optical microscope. Chip morphology was studied and chip dimensions were analyzed. Chip sample examination indicated the phenomenon of brittle fracture.

Table 5.11 Chip size comparison

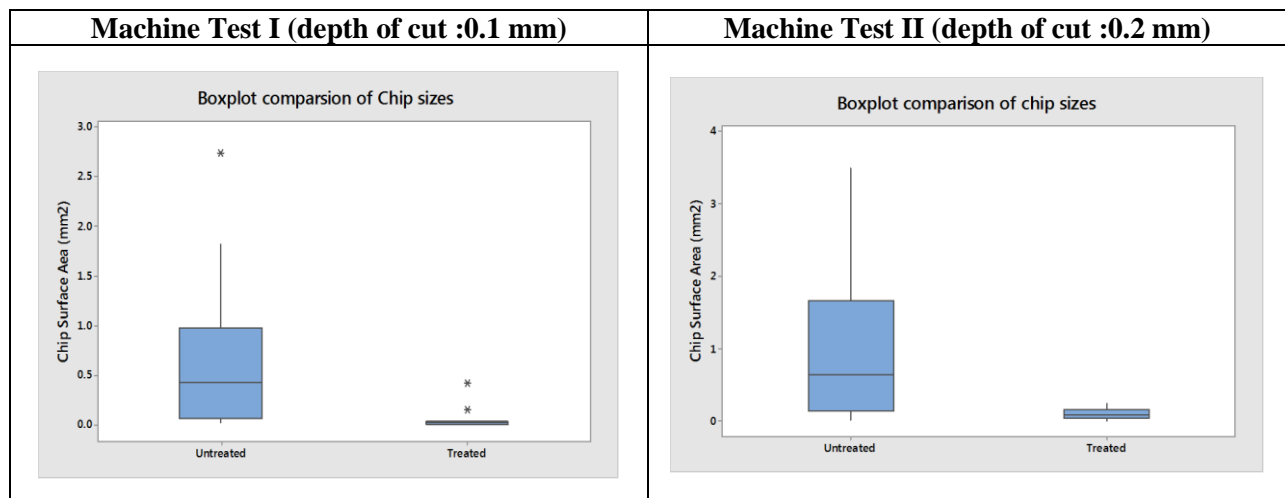


Table 5.11 shows that large chips were generated when machining untreated samples. Chips collected from treated sample experiments were relatively small and of mostly uniform geometry. In addition, chip sizes increased with the material removal rate. The mean chip surface area from untreated sample Machining Test I was approximately 0.4 mm^2 . The mean chip surface area from untreated sample Machining Test II was approximately 0.75 mm^2 . The mean surface areas of treated machining chip samples were relatively smaller and were approximately 0.01 mm^2 . Figure 5.10 shows optical images of chip samples.

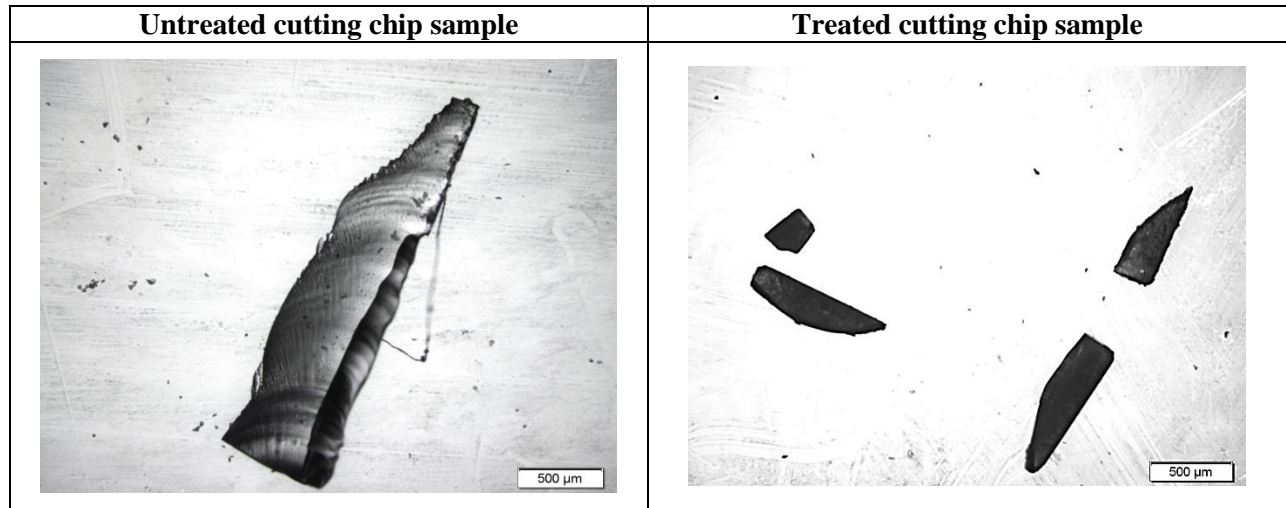


Figure 5.10 Optical images of cutting chips from machine test II (0.2 mm depth of cut)

5.3.5 Tool Wear

The cutting tool edge was studied under optical microscope before and after machining. A new cutting edge was used for each machining experiment. After machining, the tool edge was studied for wear on the rake face and the flank face of the tool.

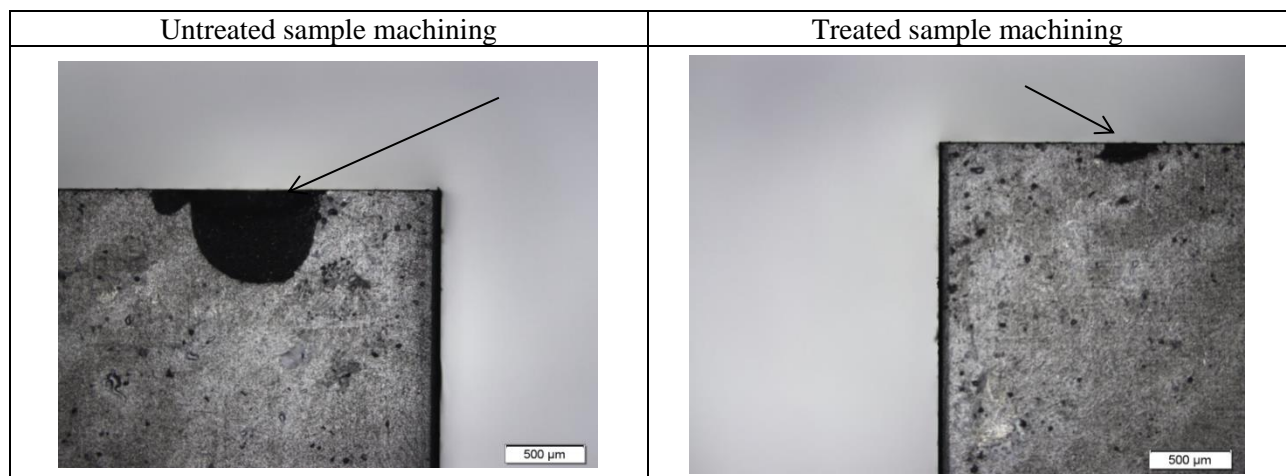


Figure 5.11 Optical image of flank face tool wear after Machining Test II (depth of cut:0.2 mm)

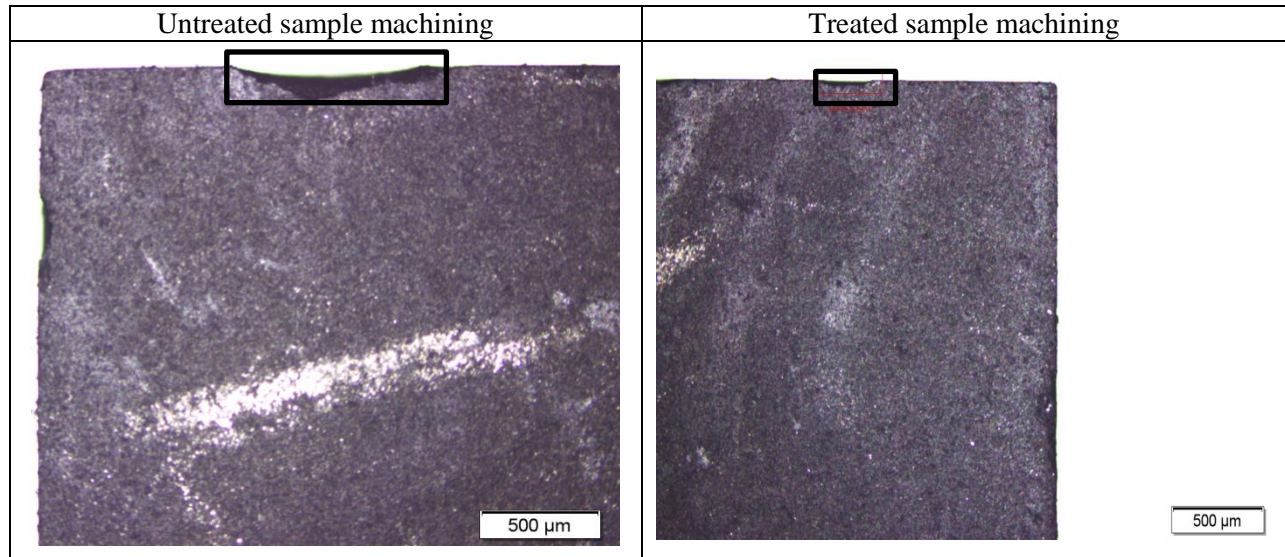


Figure 5.12 Optical image of rake face tool wear after Machining Test II (depth of cut: 0.2 mm)

Figures 5.11 and 5.12 show the flank face and the rake face of the tool after one run of machining test with 0.2 mm depth of cut. The optical images show that maximum tool wear occurred when machining untreated samples. Maximum tool wear at the flank face was measured after each cut. Because the tool edge was used for just one cut in this study, the maximum tool wear, VB_{max} is the measurement taken at the flank face of the tool after machining. Study of the cutting tool shows that there is large abrasive wear on the cutting tool upon machining untreated samples. Abrasive wear is a common phenomenon when machining brittle materials.

Table 5.12 Maximum flank tool wear

Depth of cut, mm	Maximum Flank wear VB_{max} , um	
	Treated	Untreated
0.1	88.4	302.6
0.1	68.2	210.7
0.1	98.6	193.4
0.2	180.9	640.3
0.2	253.6	743.8
0.2	228.8	589.3

Table 5.12 shows that maximum flank face wear for untreated samples was higher than that for treated samples. Maximum flank wear observed when machining untreated samples was approximately three times higher in comparison to the same observed after machining treated samples.

Chapter 6 Conclusions and Future Work

6.1 Conclusions

Machining brittle materials is a challenging task due to their hardness and low fracture toughness. A study of orthogonal machining of one such transparent brittle material, BK7 glass, was conducted with laser induced seed damages. Laser micromachining and orthogonal machining setup necessary to facilitate the material removal operation was presented. Experimental results will further help in understanding of the effects of laser induced damage on the material removal operation. The following conclusions were obtained from this study:

1. Cutting force was significantly reduced when machining laser treated samples, compared to machining untreated samples. Therefore, laser-induced damage assists the material removal process by weakening the material and working synergistically with the orthogonal machining process.
2. No subsurface damages (SSD) developed after machining laser treated samples, while subsurface cracks as deep as 1.6 mm were found for untreated samples. Because SSDs compromise part quality, laser treatment improves the surface integrity and increases the material life span.
3. The analysis of the chip samples suggested good fit between the chip size and shapes and surface defects. Chip sizes are found to increase in proportion to the material removal rate.
4. Reduction of tool wear upon machining treated samples was noted. Tooling accounts for a significant portion of machining costs especially for brittle materials. Therefore, reduced tool wear will decrease machining costs.
5. This study provided insights on laser induced damage profiles in BK7 glass, and the effects of laser micromachining conditions on the size and shape of the damage.

6.2 Future Works

1. The research should be further continued by producing laser damages in bulk transparent materials, and the effects should be analyzed.
2. Greater control over the laser treatment parameters could help achieve precise geometry. Propagation of damages beyond the intended spot when performing laser micromachining could be addressed through further studies.
3. Extension of this study to other transparent brittle materials such as fused silica could be performed. When using fused silica as a work sample, a harder tool should be chosen.

4. Extension of this methodology to other machining processes, such as milling, turning and drilling could be studied.

References

1. Brow, Richard K; Schmitt, Melodie L; 2009, “A survey of energy and environmental applications of glass” , Journal of the European Ceramic Society, Vol.29(7), pp. 1193-1201.
2. Pawar,Pravin; Ballav,Raj; Kumar,Amaresh; 2015, “ A review on machining of glass materials”, IEEE conference on emerging trends in engineering, business and disaster management, Journal of emerging technology in mechanical science and engineering.
3. <http://www.glassonline.com/site/history-of-glass>
4. Axinte,Eugan;2011, “Glasses as engineering materials: A review”, Materials and Design, vol.32(4), pp.1717-1732.
5. Osborne, Mike;2004 , “Glass machining leaps into the 21st Century: laser-based machining systems are bringing routine production to an area previously characterized by a craftsman's skill. New and complex glass geometries are opening exciting applications for a well-characterized and inexpensive material.(Materials Processing)”, Laser Focus World, Vol. 40(5), p.S4(4)
6. Khan,A.A ; Haque,M.M ; 2007 ,” Performance of different abrasive materials during abrasive water jet machining of glass” , Journal of materials processing technology, v191(1-3), pp 404-407.
7. Zeng, Xianwu ; Gan X, Yong; 2011, “ A review on grinding technologies for glass machining”, International journal of abrasive technology; v4(3); pp 223-229.
8. Zhao, Q., Liang, Y., Stephenson, D and Corbett, J. (2007) ‘Surface and subsurface integrity in diamond grinding of optical glasses on tetraform ‘C’’, International Journal of Machine Tools & Manufacture, Vol. 47(14), pp.2091–2097.
9. Chen, M. J., Li, D. and Dong, S. (2002) ‘Research on a large depth-to-diameter ratio ultra-precision aspheric grinding system’, Journal of Materials Processing Technology, Vol. 129(1–3), pp.91–95.
10. Zhengfeng, Wang ; 2001 ,” Chemical Mechanical Planarization “ Joining technology group, Process technology division.
11. Tian Y.B; Ang Y.J ; Zhong Z.W ; Xu . H ; Tan R ; 2013 ,” Chemical mechanical polishing of glass disk substrates : Preliminary Experimental Investigation” , Materials and Manufacturing processes; v28 ; pp488-494.
12. <http://what-when-how.com/nanoscience-and-nanotechnology/atomic-force-microscopy-simulation-of-interaction-forces-in-cmp-applications-part-1-nanotechnology/>

13. Saleh, T; Rahman M Sazedar ; Rahman H.S Lim; 2007, “ Development and performance evolution of an ultraprecision ELID machine” Journal of materials processing technology; v192-193;pp287-291.
14. Ohmori, H., Katahira, K., Nagata, J., Mizutani, M. and Komotori, J. (2002) ‘Improvement of corrosion resistance in metallic biomaterials by a new electrical grinding technique’, Annals of the CIRP, Vol. 51, No. 1, pp.491–494.
15. Stephenson, D.J., Sun, X. and Zervos, C. (2006) ‘A study on ELID ultra precision grinding of optical glass with acoustic emission’, International Journal of Machine Tools & Manufacture, Vol. 46, No. 10, pp.1053–1063.
16. Rahman, M ; Kumar A Senthil ; Biswas I ; 2009 ,” A review of Electrolytic In-Process Dressing (ELID) grinding “ , Key Engineering Materials; Vol 404; pp45-49.
17. Cakir, O ; yardimeden , A; Ozben, T ; 2007 ,” Chemical machining” , Archives of material science and engineering ; v28(8) ; pp499-502.
18. Belkhir, N ; Bouzid, D; Herold, V ; 2007 , “ Corelation between the surface quality and the abrasive grains wear in optical glass lapping” ; Tribology International ; v40(3); pp498-502
19. Neo,Wee Keong; Kumar,A.Senthil ; Rahman, Mustafizur; 2012 , “ A review on the current research trends in ductile regime machining”, international journal of advanced manufacturing technology , v63(5-8), pp 465-480.
20. Moriwaki, Toshimichi ; Shamoto,Eiji ; Inoue,Kenji ; 1992, “Ultraprecision ductile cutting of glass by applying ultrasonic vibration” , v41(1),pp 141-144.
21. Patten A John ; Muralidhar K Ghantasala; Ravindra Deepak; 2011 , “The effects of laser heating on the material removal process in Si and SiC” , Proceedings of 2011 NSF Engineering research and Innovation Conference, Atlanta.
22. An, Quiglong; Ming , Weiwei ; Ming Chen; 2015 ,” Experimental Investigation on Cutting Characteristics in Nanometric Plunge-Cutting of BK7 and Fused Silica Glasses” , Materials, v8(4); pp1428-1441
23. Jagannatha,N; Somashekhar S Hiremath; Sadashivappa, K; Arun K.V; 2012, “Machining of soda lime glass using abrasive hot air jet: An experimental study” , Machining science and technology, v16(3); pp459-472
24. El-Domiatty, A; Abd el-Hafez H.M; Shaker M.A ; 2009 , “Drilling of glass sheets by abrasive jet machining”;World acadamy of science , engineering and technology ; v(56);pp61-67.
25. Fan, J.M; Wang,C.Y; Wang, J; 2009 ,” Modelling the erosion rate in micro abrasive air jet machining of glasses” , v266(9-10);pp968-974.

26. Hunag, C.Z ; Wang, J; Feng,Y.X; Zhu,H.T; 2006,” recent development in abrasive water jet machining technology”,v315-316;pp396-400.
27. Bertolini ,A ; Beverini, N ; Lago G Dal ; Desalvo R ; Fidecaro F; Francesconi F; Francesconi M; Omincioli G ; 2010,” A 5-axis CNC ultrasonic cutting machine : design and preliminary test”
28. Choi,J.P; Jeon, B.H; Kim, B.H; 2007,” Chemically assisted ultrasonic machining of glass”, Journal of materials processing technology; v191(1-3); pp153-156.
29. Baek,Dae kyun ; Ko, Tae Jo ; Yang, Seung Han ; 2013,” Enhancement of surface quality in ultrasonic machining of glass using a sacrificing coating”, Journal of materials processing technology; v213(4);pp553-559
30. Zhang,C ; Rentsch,R; Brinksmeier E; 2005 ,” Advances in micro ultrasonic assisted lapping of microstructures in hard-brittle materials: A brief review and outlook” , International journal of machine tools and manufacture ; v45(7-8);pp881-890.
31. Han,Min-Seop ; Min,Byung-Kwon ; Lee,Sang,Jo ;2011,” micro electrochemical discharge cutting of glass using a surface textured tool”, CIRP journal of manufacturing science and technology;v4(4); pp362-369.
32. Basak, Indrajit; Ghosh, Amitabha ; 1997 ,” Mechanism of material removal in electrochemical discharge machining : a theoretical model and experimental verification”, Journal of materials processing technology; v71(3);pp350-359.
33. Cheng,Chih-Ping ; Wu,Kun-Ling ; Mai,Chao-Chuang ; Hsu, Yu-Shan; Yan, Biing-Hwa; 2010,” magnetic field assisted electrochemical discharge machining”, Journal of micromechanics and micrengineering; v20(7); 075019
34. Han , Min-Seop; Min, Byung-Kwon ; lee,Sang Jo; 2008 ,” Reduction of overcut in the electrochemical discharge machining process using a side-insulated electrode” , ICMA 2008 – International conference on smart manufacturing application; pp251-254;4505652
35. Misra , S; Yadava, V ; 2015 , “ Laser beam micromachining(LBMM) – A review” Optics and lasers in engineering ; v73; pp89-122.
36. Lei, Shuting; Pfefferkom, Frank; 2007,” A review of thermally assisted machining “ ,Proceedings of the ASME International Manufacturing Science and Engineering Conference 2007, MSEC2007.
37. Schaffer, C.B ; Brodeur, A; Gracia, J F ; Mazur, E; 2001,” Micromachining bulk glass by use of femtosecond laser pulses with nanojoule energy” , Optics letters; v26(2); pp93-5.
38. Ueda, T; Yamada, K; Oiso, K ; Hosokawa,A ; 2002,” Thermal stress cleaving of brittle materials by laser beam”, CIRP Annals – manufacturing technology; v51(1); pp149-152.

39. Barnes , Christopher ; Shrotriya , Pranav ; Molian, Pal ; 2006,” A Hybrid laser/water jet cutting process for brittle materials” , Transactions of the north American manufacturing research institute of sme; v34; pp111-118.
40. Chiu , Wei-Chong ; Endres, William J ; Thouless, M.D; 2000,” Experimental study on orthogonal machining of glass”, Machining science and technology; v4(2); pp253-275.
41. Bifano, T.G., Dow, T.A. and Scattergood, R.O. (1991) ‘Ductile-regime grinding: a new technology for machining brittle materials’, Journal of Engineering for Industry, Vol. 113, No. 3, pp184–189.
42. Arif, Muhammad; Rahman, Mustafizur; San, Wong Yoke ; 2012,” An experimental study on machining characteristics in ductile mode milling of BK7 glass “ International journal of advanced manufacturing technology; v60(5-8) ; pp487-495.
43. Arif, Muhammad; Rahman, Mustafizur ; San, Wong Yoke; 2010, “ An experimental study on microcutting of soda-lime glass by milling process” ; key engineering materials ; v 447,448; pp116-120.